Why do anaerobes like the light stimulation: Enhanced anaerobic digestion at different wavelengths under ammonia stress

Yunxin Zhu[a], Guangqi An[a], Cheng Zhang[a], Guoping Chen[b], Yingnan Yang[a]*

[a]*Graduate School of Life and Environmental Science, University of Tsukuba, 1-1-1 Tennodai, Tsukuba, Ibaraki 305-8572, Japan*

[b]*Research Center of Functional Materials, National Institute for Materials Science,1-1 Namiki, Tsukuba, Ibaraki 305-0044, Japan*

* Corresponding author:

Tel/Fax: +81 29 8534650

E-mail address: yo.innan.fu@u.tsukuba.ac.jp (Y.Yang)

Abstract

Strengthening microbes with light during anaerobic digestion (AD) has emerged as a promising approach for effective waste-to-energy conversion, yet the underlying mechanisms remain elusive. This study delved into the complexities of microbial behavior, metabolic pathways, and digestion efficiency to explore the light-stimulating effects of various wavelengths (blue, green, red and mixed wavelengths) on AD under ammonia stress. Different light wavelengths induced distinct responses in anaerobic consortia and cell metabolism. Blue and green light impacted the Energy and Methane metabolism, while red light regulated the Cell cycle and motility-related genes. Although *Methanosarcina* dominance was observed across all the lighted groups, the dominant pathway shifted from hydrogenotrophic to acetoclastic methanogenesis specifically under the mix-color lighting. This characteristic was attributed to the collaborative effects of short and long wavebands, enhancing the diversity of microflora and triggering the cellular processes more effectively. Moreover, the enrichment of syntrophic bacteria and *Methanosarcina* (91.3% of archaeal community) facilitated the complete degradation of organic acid and outperformed methanation under mixed wavelengths. Furthermore, metagenetic predictions elucidated that critical metabolic processes regulating organic conversion (Carbohydrate metabolism), microbial response (Signal transduction, Membrane transports system) and cross-population cooperation (Quorum sensing) were significantly activated under the mixed wavelengths. Notably, the mixed-wavelength light stimulation upregulated a c-type cytochrome-mediated interspecies

communication, fostering an energy-conserving bionetwork via electronic signals. From the academic to the practical viewpoint, this study unveiled the mechanisms and potential of a visible light-stimulated system for waste-to-energy conversion, highlighting the feasibility of sustainable sunlight-mediated waste management and energy recovery on a larger scale.

Keywords: Visible light stimulation; Spectral effect; Ammonia-rich anaerobic digestion (AD); Metagenomic analysis; Interspecies electron transfer (IET)

1. Introduction

Global challenges such as environmental deterioration and energy depletion have reached an alarming pace, casting a shadow over human health and societal advancement [1,2]. Sustainable management of waste through anaerobic digestion (AD) holds the promise to minimize pollutant emissions meanwhile harness renewable energy (e.g., H_2 and CH_4) [3]. AD process involves complex stages—namely, hydrolysis, acidogenesis, acetogenesis and methanogenesis—which converts macromolecular compounds into bioenergy with concomitant generation of volatile fatty acids (VFAs) as secondary products. Indeed, the stable operation of AD calls for a delicate balance between the above steps, which necessitates a collaborative effort between diverse bacteria and methanogens for catalyzing the optimal performance [4]. However, multiple inhibitory factors in AD, e.g., ammonia toxicity (when ammonia levels exceed 1500 mg/L) accompanying with inhibited metabolic activity, impaired microbial structure and undesirable VFAs accumulation, generally undermines the efficiency of bioconversion process and waste treatment [5,6]. Thus, searching a pragmatic and efficacious approach to improve the digestion performance stands as a pressing need.

The utilization of illumination to stimulate anaerobic microorganisms has recently emerged as an innovative practice to promote the conversion of organics into CH_4, which challenges the traditional notion that AD predominantly occurs in darkness. Early studies on light-enhanced AD were conducted by Sawayama et al, who observed that light exposure improved the removal efficiency of total organic

carbon (TOC) and toxic ions (such as ammonia, phosphate, and sulfate) in up-flow anaerobic sludge blanket [7,8]. Besides, the introduction of incandescent lighting yielded a two-fold enhancement in biogas and CH_4 production compared to dark AD [9,10], which were likely due to the photoactivating effect of light [11,12]. Multiple lines of evidence propounded that light stimulation assisted to shorten the lag phases and increase the biogas production, thereby significantly advanced the AD operated in different modes [13–15]. In particular, light stimulation has demonstrated a pronounced efficacy in overcoming ammonia-induced inhibition in AD, due to its effectiveness in activating anaerobes and strengthening the cell-cell syntrophic communication [16–18]. Furthermore, extensive researches have highlighted the practical potential of light stimulation strategies in the context of fostering large-scale waste-to-energy conversion [19–21]. Among the diverse light sources, solar irradiation from nature is an attractive alternative to artificial lighting, as it offers a readily available and environmentally benign option for economically viable scaled-up systems. However, the limited knowledge about the sunlight-stimulating effect and the internal mechanisms of light-related microbial nexus in AD necessitates the further exploration.

Light plays a vital role in the lifestyles of all living beings on earth. Variations in light conditions (e.g., light intensity, exposure time and wavelength) could regulate microbial behavior and result in the different performances. For instance, light intensity influenced the framework of microbial community [21], while the illumination time exhibited a distinct relation with cell availability and activity [13]. A

model-based analysis quantitively predicted the effect of light conditions on CH_4 yield, revealing that light could alter the metabolic pathways, microbial community and sludge properties [20]. However, previous efforts into the role of light have primarily gravitated toward light quantity (namely, intensity and time), while little is known about light quality, specifically, the light wavelength. In fact, wavelengths associated with specific light color might have distinct effects on microbial behavior. Within the board solar spectrum, ultraviolet (UV) light with high photon energy might cause photochemical damage to the cells, while near-infrared/infrared lights associated with long-wave spectrum have significant thermal effects [22]. In contrast, the visible spectrum (400–800 nm), which accounts for a substantial 50% of solar energy, holds the potential to significantly impact the microbes and their propensities for proliferation [20]. As reported, red light could regulate the enzymatic activity in respiratory chain [23] and bacterial proliferation [24]. A beneficial effect of low-intensity blue light (390–540 nm) on CH_4 production was documented [9], while certain investigations concurrently unveiled its negative impact on specific archaebacteria and enzymes [25,26]. In addition, previous investigations on spectral effect were mostly conducted under distinctive wavelength in pure-culture system, very few studies have been focused on the mixed microflora in ammonia-stressed AD bioprocess. Moreover, the regulated metabolic pathways and syntrophic features of light-activated community in response to different wavelengths remains unknown. Recently, bioinformatics analysis, including taxonomic trees and the Kyoto Encyclopedia of Genes and Genomes (KEGG) pathway could track the changes in

119 microbial network [27], which is a potential way for better understanding the
120 mechanisms involved in light-stimulated AD.

121 In this study, the objective was to explore the impact of different wavelengths on
122 light-assisted anaerobic digestion (AD) under ammonia stress. To simulate the diverse
123 wavelengths within the visible solar spectrum, the energy-efficient light-emitting
124 diodes (LEDs) were utilized as a light source. Specifically, this study involved: (1)
125 comparing the performance of AD at short, medium, long, and full visible
126 wavelengths; (2) examining the structure and properties of mixed consortia
127 characterized by various light colors; and (3) delving into the mechanism on the
128 wavelength-regulated metabolic pathways and syntrophic association. To the best of
129 our knowledge, this is the first study to elucidate the light-stimulating mechanism via
130 metagenomic analysis of microbial profiles and metabolic routes. The obtained results
131 could provide insight into the internal changes in light-assisted anaerobic bioprocesses
132 from academic point, and further contribute to guiding the practical engineering of a
133 solar-integrated bioprocess for the treatment of ammonia-rich feedstock.

134 **2. Materials and methods**

135 **2.1 Seed sludge and substrate**

136 Seed anaerobic sludge was obtained from a mesophilic sewage treatment plant in
137 Ibaraki prefecture, Japan. After being collected in an airtight container, sludge was
138 stored at 4ºC for use until no more biogas was produced. Before use, anaerobic pre-
139 inoculation under 55 ± 1ºC was conducted in fermentation reactor (500 mL, SIBATA)
140 with collected seed sludge (20 v/v%) and diluted synthetic medium (80 v/v%). During

two-week preculturing, the synthetic medium consisted of glucose (2.5 g/L), sodium acetate (2.5 g/L), yeast extract (200 mg/L), NH_4Cl (200 mg/L) and KH_2PO4 (16 mg/L) was dissolved in trace element solution (50 mL/L) and then added into reactor every two days. The chemical composition of trace mineral solution was recorded in a previous study [18].

2.2 Anaerobic fed-batch fermentation under light of different colors

In order to assess spectral effects on light-assisted AD, fermentation assays were carried out under LED illumination with different light colors. Blue, green, and red were selected as the three primary light colors to present the short (400−500 nm), medium (500−600 nm), and long (600−800 nm) wavebands of visible light, respectively. Moreover, a polychromatic white LED light (400−800 nm) was employed as a comparative treatment to simulate the entire visible spectrum. According to previous studies [13,17], daily illumination of 60 mins was applied to each reactor with intermittent stirring (100 rpm with 3 mins on and 12 mins off) to ensure the homogenous light stimulation. Each lighted reactor had a light intensity of 5 ± 1 W/m^2 with monochromatic LEDs (namely, Blue, Green and Red) and 17 ± 2 W/m^2 with polychromatic LED (namely, Mix), which was the sum of the individual monochromatic lights. After lighting, the reactors were placed in darkness immediately. The control reactor (Dark) was operated in dark, which was wrapped entirely in aluminum foil to keep out all light. The schematic diagram of reactor and spectrum of LED source were depicted in Fig. S1.

Sequential fed-batch assay was conducted for three cycles, including the start-up

period (5 days), cycle 1 (4 days) and cycle 2 (3 days). Each treatment (100 mL) was initially inoculated with acclimatized digested sludge (16 mL) and synthetic medium (64 mL). After adjusting the initial pH to 7.0 ± 0.2, each reactor was then purged with N_2 gas for 3 min, sealed immediately to ensure anaerobic condition and then kept in a thermophilic incubator. Biogas production was monitored daily, and when the CH_4 production ceased, the supernatant liquid was replaced by a new substrate solution. The NH_4Cl was adopted into each reactor to maintain an ammonia-stress environment of 2500 mg/L.

2.3 Analytical methods

The biogas composition was analyzed by gas chromatography (GC-8A, SHIMAZU, Japan). Sampled digestate (2 mL) was centrifuged and filtered with supernatant for the measurement of dissolved organic carbon (DOC), VFAs and pH according to previous study [18,20]. Modified Gompertz model was performed to compare the AD performance under different light conditions, which depicted the correlation between the cumulative CH_4 production and the lag phase time using a sigmoid function [28]. Parameters including cumulative CH_4 production (M_{max}, mL/L) maximum CH_4 production rate (R_{max}, mL/day) and lag phase time (λ, day) were estimated using the curve fit function in *Origin 2021* software.

2.4 Microbial community and metagenomic analysis

The composition of the microbial community collected from each treatment and inoculum were quick frozen at -80℃ and stored after fed-batch assay. Illumina MiSeq paired-end sequencing (Illumina, USA) of 16S rRNA V4 regions (515F–806R) was

185 performed at Bioengineering Lab. Co., Ltd. (Kanagawa, Japan). Briefly, DNA
186 extraction with a two-step, tailed PCR approach was performed for 16S metagenomic
187 sequencing library preparation, according to the manufacturer's instruction
188 (https://www.gikenbio.com.). The prepared libraries were used for paired-end
189 sequencing with 2×300 bp reads and assembled based on QIIME2. Quality filtered
190 reads were assigned to operational taxonomic units (OTUs) (99.7% identity) using
191 taxonomic assignment against the EzBioCloud 16S database
192 (https://www.ezbiocloud.net/) [29]. Diversity analyses were performed using QIIME2
193 with default parameters. Indices of α-diversity for richness comparison (using
194 observed species and Chao1 index) and diversity comparison (using Shannon index
195 and phylogenetic diversity (PD) whole tree) were analyzed based on the size of
196 samples and normalized using sequences (no less than 10000 sequences) obtained
197 among different samples. Phylogenetic Investigation of Communities by
198 Reconstruction of Unobserved States (PICRUSt2) was used to predict the functional
199 gene products in the microbiota based on the taxonomy obtained from the
200 EzBioCloud 16S database. The gene products were classified using KEGG ortholog
201 (KO) and mapped using the KEGG Mapper (https://www.genome.jp/kegg/mapper/).

202 **2.5 Statistical analysis**

203 All experiments were repeated in triplicate. An analysis of variance (ANOVA)
204 was employed to evaluate the significance of the results, $p < 0.05$ was considered to
205 be statistically significant and $p > 0.05$ was considered to be statistically insignificant.

3. Result and discussion

3.1 AD performance under different light spectrum

The effects of light stimulation with different colors on AD performance in three-cycle fed batch were illustrated in Fig. 1 and modeled by the modified Gompertz equation (Table 1). Due to the ammonia toxicity, Dark group showed the lowest CH_4 production (Fig. 1a) and unstable CH_4 concentration (Fig. 1b), with the longest lag phase of $\lambda = 0.6–2.1$ days throughout the cyclic operation (Table 1). While under light stimulation, the cumulative CH_4 production (Fig. 1a) from the Blue, Green, Red and Mix groups were 1074 ± 75, 1126 ± 79, 1946 ± 139 and 1875 ± 131 mL/L, respectively, which were 1.77, 1.86, 3.28 and 3.10 times higher than that of Dark control (606 ± 42 mL/L). During the start-up period, Red and Mix groups exhibited the highest CH_4 concentration (86.2% and 85.0%, respectively) on day 4, followed by Blue (81.9%) and Green (75.9%) groups (Fig. 1b). While relatively lower level of 73.7% (on day 5) was observed in the Dark group. This implicated that visible light exposure could enhance methanogenic productivity under ammonia stress, and the promotion efficacy depended on the specifically spectral properties of light. Especially, Red group exhibited an outcompeting CH_4 production among all lighted groups (Fig. 1a), contributing to 4.82 folds of CH_4 cumulation (941 mL/L) on day 5 compared to the that of Dark group (195 mL/L). Generally, start-up period is considered as the rate-limiting step in ammonia-stressed AD, as it provides a prerequisite phase for the anaerobic microorganisms to acclimate to the new environment [30]. The superior performance under red lighting could be attributed to

the stimulatory effect of long-wavelength lighting on cell growth and proliferation in start-up [24,31], favoring the microbial acclimatization and CH_4 productivity. However, the stimulatory effect of sole red-light was uncapable of further sustaining in the subsequent cycles. The maximal CH_4 concentration of Red group decreased to from cycle 1 (Fig. 1b), and the maximum cumulative CH_4 production (M_{max}) under red lighting halved from 1014 mL/L (start-up) to 438 mL/L (cycle 1) and 546 mL/L (cycle 2) (Table 1). In contrast, mix-color lighting could steadily maintain the maximal CH_4 concentration at 80−85% throughout the operation (Fig. 1b), which led to steadily promoted M_{max} (628−797 mL/L) in three cycles (Table 1). Accordingly, the gap of CH_4 production between Mix and Red groups gradually minimized in following 2 cycles (Fig. 1a), achieving comparative CH_4 accumulation ultimately on day 12. These variations suggested that mix-color lighting showed better sustainability in assisting AD performance under ammonia stress, as compared to exclusive sole-color lighting. On the other hand, reactors under blue- and green-light achieved similar CH_4 productions (Fig. 1a), but a sharp decrease in M_{max} from 593 mL/L (start-up) to 489 mL/L and 123 mL/L (cycle 1 and cycle 2, respectively) was observed in the Blue group. This probably related to the high energy contained by short visible waveband might restrain the enzymatic activity and cell growth [7]. While green lighting might be favorable for improving methanogenic productivity [32], as demonstrated by the steadily increased M_{max} (172−489 mL/L) and shorter lag phase (0.2–0.7 day) in the Green group throughout the three-cycle operation (Table 1). These observations illustrated that each light color within visible range might

stimulate AD performance in different ways, and mix-color lighting ultimately resulted in a superior and stable overall performance.

3.2 Influence of light wavelengths on metabolized organic acid

As a major class of metabolic byproducts in AD, VFAs play a double-edged role in organics conversion and CH_4 production. To further dig the mystery behind the wavelength-regulated enhancement, the variations of VFAs were investigated. During start-up (Fig. 2a), all the light-treated groups exhibited lower acetate levels than that of dark group, implying the accelerated acetate consumption via the light-activated anaerobes under ammonia stress. As a critical precursor for methanogenesis, acetate (contributing to 65–70% of CH_4 production) varying in the favorable levels indicates a fine balance between acidification and methanogenesis [33]. Compared to other treatments (Fig. 2a), Red group remained apparently less acetate (807 mg/L) from day 3 (when CH_4 content > 60% in all treatments), implicating the ability of red-light on pulling the acetate conversion into CH_4 in the early stage. However, after three-cycle operation, more acetate remained in Red (476 mg/L) on day 12 among all the groups, indicating that sole red-light stimulation was unsuitable for continuous acetate-to-CH_4 conversion. This unsustainable effectiveness of red light was in consistence with reduced M_{max} in following 2 cycles (Table 1). Additionally, more propionate accumulated in Red (100–161 mg/L) on day 5, 9 and 12 (Fig. 2b), as compared to that of the Dark group (20–99 mg/L). While less propionate, butyrate and lactate were observed in the Blue and Green groups on the ultimate day of each cycle. Generally, propionate often remains unconverted in ammonia-stressed AD, owing to its

thermodynamically constrained properties and the sensitivity of acid degraders to ammonia [34]. Above findings implicated that compared to red-light stimulation, blue and green ones had better contributions in assisting the degradation of resilient VFAs under ammonia stress.

In comparison to single-color lighting, Mix group exhibited a stable acetate conversion efficiency and complete degradation of resilient VFAs throughout the operation. After 5-day acclimatization to mix-color lighting (Fig. 2), negligible acetate (0–18 mL/L) and other VFAs (0–9 mL/L) accumulated at the end of cycle 1 (day 9) and cycle 2 (day 12). This promoted degradation efficiency suggested that mix-color light stimulation had outcompeting ability on stabilizing the organic conversion efficiency under ammonia stress, as compared to other light treatment. This was in accordance with the steadily increased CH_4 production (Fig. 1a) in the Mix group throughout the operation. Conclusively, light varies in colors behaved differently in influencing the organic degradation and methanogenic performance, as each light color made distinctive contribution to process efficiency. By benefiting from the synergy of blue-, green- and red-light effects, light-assisted digester with mixed color achieved an efficient and stable organics acid conversion under ammonia stress.

3.3 Functional bacterial community under different wavelengths

Efficient organic conversion into CH_4 depends on the establishment of a delicate metabolic balance and syntrophic interactions between bacterial and archaeal communities. To explore the mystery behind the light-triggered enhancement, the bacterial communities under different light treatments were assessed firstly (Fig. 3a).

294 Compared to Inoculum, Dark group exhibited higher abundance of Petrotogals
295 (21.2%), Bacillales (23.8%) and Thermoanaerobacterales (14.8%), Hydrogenispora
296 (2.3%) and Erysipelotrichales (2.0%), which commonly abundant in ammonia-rich
297 AD [35]. While the fractions in Clostridiales (30.1%), Tissierellales (3.1%),
298 Spirochaetales (1.5%), and Anaerolinaeles (0.8%), Cloacamonas (0.5%) reduced, due
299 to their sensitivity to ammonia stress [36]. Under light treatment, above reduced
300 populations could be conserved in different ways. For examples, the abundances of
301 Clostridiales and Tissierellales, which contain efficient acetogens and sugar degraders,
302 increased to 32.3−47.9% and 3.1−4.4% under light conditions, respectively.
303 Especially under sole red-light stimulation, a remarkable enrichment of the
304 Clostridiales (47.9%) was observed. Populations in Clostridiales are characterized as
305 syntrophic acetate oxidizing bacteria (SAOB), which are known for their ability in
306 fast acetate degradation into H_2/CO_2 and contribution to hydrogenotrophic
307 methanogenesis (HM) under ammonia stress [37]. Those red light-enriched SAOB,
308 dominating approximately half of the bacterial community, could potentially assist the
309 SAO-HM pathway for fast CH_4 conversion in the Red group. This discovery
310 harmonized with the rapid degradation of acetate (Fig. 2a) and the accelerated CH_4
311 production (Fig. 1a) in the Red group during the start-up period. Besides, mix-color
312 lighting particularly increased populations in Spirochaetales (2.8%), Anaerolinaeles
313 (1.9%) and Cloacamonas (1.0%), accounting for approximately 2-fold abundances of
314 that in the Dark group (Fig. 3a). These visible light-enriched orders comprise
315 proficient syntrophic propionate and butyrate degraders [35,38,39], which agreed with

316 the negligible VFAs accumulation in Mix group until the end of cyclic operation (Fig.
317 2b).

318 Since bacteria community (order level) in Blue and Green groups showed
319 insignificant differences ($P > 0.1$) with Dark group, to unveil the intricate relations
320 between light and bacterial community, a heatmap with cluster analysis on dominant
321 genera was generated. As shown in Fig. 3b, blue light treatment preserved the
322 fermentative genera of *Defluviitoga*, *Coprothermobacter* and *Haloplasma*, which
323 were specialists in hydrolysis and acid degradation during ammonia-rich AD [40–42].
324 Besides, blue and green light promoted the co-growth of the hydrolytic populations
325 (*GU455315*, *Defluviitalea* and *Tepidimicrobium*), acid-producing bacteria (*Bacillus*)
326 and H_2 producers (*DQ887962* from Hydrogenispora). These enriched communities
327 were in alignment with fast VFAs degradation (Fig. 2b) under blue and green light, as
328 compared to that of the Dark group. On the other hand, red light stimulation
329 exclusively activated the genus *Thermoclostridium*, which was hardly observed under
330 other light treatments (Fig. 3b). *Thermoclostridium* harbors the ability in degrading
331 various types of sugars into acetate/ethanol and converting the resulting acetate into
332 H_2/CO_2 [43]. Consequently, the fermentative versatility of *Thermoclostridium* could
333 expedite the conversion of biogas from organics, which harmonized with the rapid
334 degradation of acetate (Fig. 2a) and surged CH_4 production (Fig. 1a) in the Red group
335 during start-up period. However, this advantage in turn restricted the VFAs
336 conversion under red light (Fig. 2b), probably due to the reduced the competitiveness
337 of syntrophic VFAs degrading bacteria.

Unlike single-color light that enriched specific fermentative bacteria, mix-color light stimulation had better control on balancing the bacterial structure for syntrophic metabolism. In the Mix group (Fig. 3b), the clustered ammonia-repressed genera *Tepidimicrobium*, *AJ009469*, *AF402980*, *Cloacamonas*, *Rectinema* and *Clostridium* encountered a remarkable recovery. *Tepidimicrobium* (order Tissierellales), which is particularly suited for sugar and protein fermentation into acetate under high ammonia concentrations, commonly associates with the growth of SAOB [33,44]. Genera *AJ009469* (order Anaerolinaeles) and *Cloacamonas* (order Cloacamonas) were well-documented as the "semi-syntrophic" microorganisms involving in fermenting VFAs (e.g., propionate and butyrate) into acetate and H_2/CO_2, and mutually cooperating with HM to produce CH_4 [45]. Conventionally, ammonia stress readily inhibits the growth of syntrophic bacteria, leading to VFAs accumulation. Moreover, the thermodynamically unfavorable nature of resilient VFAs can exacerbate acid pressure and lower pH, restraining the methanogenic performance [46,47]. However, mixed-color lighting could trigger the revival of these syntrophic bacteria and thus favor the conversion of organic acids, providing ample substrate for methanation. This observation was coincidence with the minimal detection of VFAs in the Mix group at the end of the operation (Fig. 2b). Furthermore, genera *AF402980* and *Rectinema* (both belonging to order Spirochaetes), along with *Clostridium* (order Clostridiales) are recognized as key SAOB during AD but with high ammonia sensitivity [48]. By combining the strengths of different wavelengths, mix-color lighting provided a comprehensive stimulation on the above SAOB and assisted them in resisting

ammonia stress. Another intriguing result found in the Mix group was the exclusive enrichment of the genera *Anaerobacillus* and *Lysinibacillus*, which showed low abundance in the Dark group. *Anaerobacillus* is an obligate anaerobic diazotroph capable of nitrogen fixation and growth without external sources [49], and *Lysinibacillus* exhibits potential as a plant growth bio-stimulant due to its nitrogen bioaccumulation abilities [50]. The substantial enrichment of two genera indicated that mixed-color lighting could facilitate nitrogen utilization and ammonia assimilation. Therefore, the evenly enriched bacterial community in the Mix group, including ammonia-sensitive hydrolyzers, VFAs degraders, acetate oxidizers and ammonia degraders, led to a diversified and balanced bacterial community for effective fermentation.

3.4 Effect of different wavelengths on methanogenic microflora

The dominant methanogens were characterized to further reveal the visible light-induced changes on methanogenic microflora (Fig. 4a). Remarkably, *Methanosarcina* prevailed across all light-treated groups, as its abundance increased from 49.6% to 70.7%, 77.9% and 75.3% in Blue, Green and Red groups, respectively, and reaching an astounding 91.3% in the Mix group. However, the richness of strict hydrogentrophic methanogens (e.g., *Methanoculleus thermophilus* and *Methanothermobacter thermophilus*) experienced a sharply decrease under the single-color (19.1−26.0%) and mix-color lighting (1.7%), as compared to that of 32.2% in the Dark group. Generally, hydrogenotrophic methanogens often dominate in ammonia-stressed AD, and they could cooperate with SAOB for the utilization of

382 acetate-derived H_2/CO_2 into CH_4 [51]. However, the energetically unfavorable feature
383 (ΔG_0' = + 104.6 kJ/mol) of SAO pathway usually results in limited CH_4 productivity,
384 as compared to conventional acetoclastic methanogenesis (Table 2) [52]. In contrast,
385 the light-induced enrichment of *Methanosarcina* spp. might be favorable to relieve
386 this limitation. This methanogenic genus employs various pathways (acetoclastic,
387 hydrogentrophic and methylotrophic) for CH_4 production, allowing it to thrive under
388 stressful conditions and utilize the remained substrates [53]. Besides, the
389 electroactivity and clustered growth feature of *Methanosarcina* spp. enhances its
390 competitiveness in syntrophic associations via interspecies electron transfer (IET),
391 which is a more thermodynamically favorable path compared to the conventional
392 interspecies H_2 transfer (IHT) for CH_4 production [54]. By capitalizing on these
393 advantageous traits, the substantial enrichment of *Methanosarcina* under light with
394 different wavelengths contributed to better methanogenic performance, particularly
395 under mix-color lighting. Besides, a marked resurgence of *Methanosaeta spp.* was
396 demonstrated under mixed-color lighting (from 2.0% in Dark to 4.7% in Mix), which
397 also exhibited low richness (1.6–2.4%) in monochromatic light groups (Fig. 4a).
398 *Methanosaeta* spp. is known to be highly ammonia-sensitive due to the mono-
399 metabolic trait on acetate and rod-shaped cell morphology [55]. While the
400 unprecedented recovery under mix-color lighting highlighted the potent role of
401 mixed-wavelength lighting in photo-reactivation of ammonia-sensitive methanogens.
402 The possibility of methanogens to undergo photo-repair can be attributed to the
403 presence of deazaflavin and its derivatives in archaea, which serves as chromophores

for the photo-reactivating enzyme [56]. Consequently, the effective recovery of acetoclastic *Methanosaeta* spp. and predominance of robust *Methanosarcina* spp. under mix-color light stimulation contributed to diversified methanogenic pathways for outcompeted performance across the light treated groups.

Based on the obtained bacterial and archaeal community, light with varying wavelengths contributed differently to microbial diversity and structure. To further prove the above findings, alpha diversity metrics, including observed species, Chao1, PD whole tree and Shannon within the digestate samples were assessed (Fig. 4b−e). As estimators of microbial richness [57], indexes of observed species and Chao1 were found to be highly increased in the Mix group, as compared to that of Dark group (Fig. 4b−c). Comparatively, insignificant influence was given by sole-color light. This suggested that mix-color light stimulation had better control on promoting the microbial abundance under ammonia stress. Besides, microbial diversity was also profoundly affected by mix-color lighting, as demonstrated by the higher levels of PD whole tree obtained in the Mix group (65.5) than that of Dark group (Fig. 4d). Moreover, Shannon index that measures the species evenness increased to 4.8–5.0 under single-color lighting, and further recovered to 5.1 by mix-color lighting. Generally, higher species evenness implies the robustness and functional stability of biological system to adapt to the undesirable environment [58]. Compared to no light or sole-color light, mix-color light stimulation exerted better control in regulating a balanced microbial structure, resulting in higher diversity and stability for mitigating the ammonia stress. Consequently, the light-activated anaerobic community was

capable of sustaining a stable and superior AD performance during the three-cycle operation in the Mix group.

3.5 Variation of metabolic pathways under different wavelengths

3.5.1 Microbial response and behaviors to different light wavelengths

To unveil mechanisms behind the augmented light effects, bioinformatic analysis on functional genes was performed with KEGG mapper, and the relative abundance of predominant genes at level 3 was depicted in Fig. 5. Cluster analysis revealed that the Dark group displayed a closer association with the Blue and Green groups, followed by Red and Mix groups. This observation highlighted that the mix-color illumination had a more potent regulatory impact on metabolic pathways compared to the single-color light. Specifically, mix-color lighting significantly upregulated the genes encoding processes that involved in organic carbon conversion, including Pyruvate Metabolisms, Propanoate Metabolisms, Butanoate Metabolisms, Fatty acid Biosynthesis and Degradation. Additionally, the Membrane transport, Signal transduction and Quorum sensing (QS) involved genes were highly up-regulated in the Mix group. Phosphotransferase system (PTS) and Bacteria secretion system are crucial for sugar uptake and proteins translocation across membranes [59,60], and Two-component system enables microbes to sense environmental cues and triggers a corresponding response mediated by a regulatory protein [61]. The elevated expression of the above genes indicated that mixed-color activated anaerobes were capable of sensing light signals via membrane-bound enzyme, and thus stimulated the cross-membrane transport for substrate uptake and metabolites release. Moreover, QS

448 governing the population-level behavior (e.g., microbial communication, bacterial
449 aggregation and sludge formation), plays an important role in syntrophic community
450 for effective bioconversion [62]. Consequently, mix-color light stimulation not only
451 regulated cell metabolism for carbon conversion, but also the populations' behaviors
452 for cell-cell communication and syntrophic cooperation.

453 Comparatively, single-color light stimulation distinctively modulated the specific
454 cellular behavior with different wavelengths. Compared to the Dark group, blue and
455 green light stimulation particularly upregulated genes encoding Glycolysis for
456 carbohydrate uptake and Methane metabolism for bioenergy conversion, two critical
457 processes for CH_4 production. Moreover, blue and green light with higher photon
458 energy could penetrate deeper into the cell and influence genetic processes, including
459 RNA transcription, DNA replication and Nucleotide excision repair. These processes
460 ensured an efficient genetic information processing for proteins synthesis (e.g.,
461 functional enzymes) [47]. On the other hand, red light upregulated genes involved in
462 cellular-level activities, including Cell cycle, Bacterial chemotaxis and Flagellar
463 assembly. Cell cycle governs biomass growth and death, while Bacterial chemotaxis
464 and Flagellar assembly regulate bacterial survival and motility in dynamic
465 environments [62]. Under stressful condition, motile anaerobes could sense changes
466 in chemical surroundings (e.g., light stimuli, ammonia levels, or substrate availability),
467 and then assemble flagella and navigate towards favorable environment [63]. Thus,
468 red light-triggered enhancement of cellular activity and motility might empower
469 anaerobes to rapidly acclimatize and utilize substrate for efficient digestion. This

470 further explained the boosted CH_4 production and acetate consumption in the Red
471 group during the startup phase.

472 **3.5.2 Light-regulated metabolic pathway for CH_4 production**

473 Among functional categories, Carbohydrate, Energy and Lipid metabolism
474 played a pivotal role in AD, which involves diverse biochemical processes responsible
475 for breaking down organic substances to produce bioenergy. In Carbohydrate
476 metabolism (Fig. S2a), glucose undergoes initial conversion through Glycolysis, and
477 the resulting pyruvate can be either transformed into acetyl coenzyme A (Acetyl-CoA)
478 through Pyruvate metabolism, or into lactate for biomass growth. In most cases, the
479 generated acetyl-CoA may further convert into acetate, butyrate and propionate,
480 depending on the involved microorganisms and environmental conditions. Finally, the
481 syntrophic bacteria degrade the generated VFAs via Butanoate and Propanoate
482 metabolism, leading to the production of acetate and H_2/CO_2. Compared to Dark
483 group, blue and green light stimulation evidently upregulated genes associated with
484 Glycolysis and Butanoate metabolism (Fig. 5), while higher gene expressions linked
485 to Pyruvate, Propanoate and Butanoate metabolism were detected in the Mix group.
486 These results in aligned with the highly enriched hydrolytic and fermentative bacteria
487 under blue and green light, and significantly recovered VFAs degraders under the
488 mix-color light (Fig. 3b). Despite red light stimulation down-regulated the most
489 pathways involved in Carbohydrate metabolism (Fig. 5), it notably increased the
490 genes expression involved in M00579: acetyl-CoA → acetate (Fig. S2b), which
491 contributed to efficient acetate conversion and degradation.

The generated fermentative byproducts (e.g., acetate, H_2/CO_2 and methanol) were then traversed through distinct pathways in Methane metabolism to culminate in CH_4 generation (Fig. 6a). Compared to Dark group, Blue and Green groups exhibited a significant upregulation on Methane metabolism, while similar level was observed in the Red and Mix groups (Fig. 5). To delve deeper into short wavelength-enhanced methanogenesis, the abundances of genes encoding pivotal enzymes for each methanogenic pathway were analyzed. Three methanogenic pathways were detected (Fig. S3), including CO_2 reduction in HM (M00567), acetate decarboxylation in AM (M00357), methanol conversion in methylotrophic methanogenesis (MM) via M00356 [64]. Within acetate decarboxylation, vital enzymes including acetate kinase (*ackA*, ①EC:2.7.2.1) and phosphate acetyltransferase (*pta*, ②EC:2.3.1.8) manage the conversion of acetate to acetyl-CoA (Fig. 6a). Subsequently, acetyl-CoA is transformed into Methyl-HSPT (a key juncture in methanogenesis) via the catalysis of acetyl-CoA decarbonylase/synthase (*cdhC*, ③EC:2.3.1.169) [64]. Genes coded *pta* displayed 24% increments under red illumination as compared to the Dark group (Table S1). This result was likely correlated with the prevalence of *Methanosarcina*, as it is a pathway unique to *Methanosarcina* which is distinct from acetotrophic *Methanosaeta* [65]. Strikingly, compared to the Dark group, gene abundance of *cdhC* increased by 84%, 74%, 14% and 23% in Blue, Green, Red and Mix groups, respectively. The reaction mediated by *cdhC* presents a pivotal step in acetoclastic methanogenesis and was reported to be highly sensitive to ammonia toxicity [66]. Accordingly, the substantial upregulation of this ammonia-sensitive enzyme under

visible light stimulation was likely to explain the enhanced CH_4 productivity in light-assisted system. Since individual wavelength distinctly contributed to activating the acetate decarboxylation pathway, the absence of any wavelength might result in suboptimal methanogenic performance.

Generally, acetoclastic methanogens exhibit higher susceptibility to ammonia toxicity, consequently prompting a shifted pathway from AM to HM in methanogenic community. Under blue and green lighting, CO_2 reduction (reaction ④−⑦) was further elevated compared to that of Dark (Fig. 6b), potentially due to the ability of light-enriched *Methanosarcina*'s in H_2 utilization. In this genus, HM commences with the H_2- and MFR-dependent reduction of CO_2 to formyl-MFR [65], facilitated by formylmethanofuran dehydrogenase (*fmd*), a key catalyst for the initial step of H_2 utilization. Compared to Dark, *fmd* gene abundance surged by 61% and 35% in the Blue and Green groups, respectively (Table S1). Successively, the formyl group transfers to H_4SPT, progressing a stepwise reduction to yield methyl-H_4SPT, which powered by the electron (e^-) derive from reduced F_{420} ($F_{420}H_2$). In parallel, enzymes like methenyltetrahydromethanopterin cyclohydrolase (*mch*), methylenetetrahydromethanopterin dehydrogenase (*mtd*), and coenzyme F_{420}-dependent 5,10-methylenetetrahydromethanopterin reductase (*mer*) experienced a respective gene expression increase of 54%, 64% and 50% in the Blue group, and 28%, 35% and 18% in the Green group, respectively (Table S1). On the other hand, members in *Methanosarcina* are capable of metabolizing methylated C1 compounds (e.g., methanol and methylamines) in the absence of H_2 [67], known as MM. In this

pathway, corrinoid protein mediates the transfer of methyl groups from methylated C1 compounds to HS-CoM, yielding Methtyl-CoM (reactions ⑧–⑨, Fig. 6b). Due to the lower abundance of *Methanosarcina* in Dark, gene abundance linked to MM-involved enzymes remained modest (Fig. 6b), whereas light stimulation markedly upregulated these genes. This observation affirmed the effectiveness of visible light stimulation in driving H_2- and methanol-utilizing methanogenesis, probably associated with light-enriched *Methanosarcina*.

At the intersection of AM and HM (Fig. 6a), methyl group of Methyl-HSPT is transferred to HS-CoM via *mtr* (a membrane-bound methyltransferase), generating Methtyl-CoM (⑩EC: 2.1.1.86). Subsequently, the reduction of methyl-CoM to CH_4 occurs via *mcr* (⑪EC: 2.8.4.1), accompanied with mixed disulfide formation (CoM-S-S-CoB) and e^- receipt from coenzyme B [68]. Reversely, the CoM-S-S-CoB could be transformed back to coenzyme M and coenzyme B by a composite heterodisulfide reductase (*hdr*) with the assistance of F_{420} (⑫EC: 1.8.98.1). Both of *mtr*, *mcr* and *hdr* experienced a remarkable upregulation by 59%, 39% and 58% in Blue, and 34%, 8% and 37% in Green, respectively (Table S1). This pronounced impact of light stimulation concentrated in the range of 400–500 nm (blue-green wavelength) likely related to the light-absorbing ability of methanogenic chromophores. There are at least two known chromophores absorbing visible light found in methanogens: coenzyme F_{430} (a *mcr* cofactor), a novel nickel-containing corphin that peaks at 430 nm [69], and coenzyme F_{420} (an electrons carrier), a deazaflavin that maximally absorbs at 420 nm [25]. As shown in Fig. S3, blue and green light could effectively

558 excite genes coding for F_{420} biosynthesis compared to the dark control. Moreover, this
559 excitation suggested that the higher energy inherent in short bands photons not only
560 activated the membrane-bound enzymes (e.g., *hdr*), but also traversed the cell
561 membrane to excite the cofactor in cytoplasm (e.g., coenzyme F_{420}). Thus, the
562 efficacy of light stimulation, particularly in short visible wavelengths, conferred
563 significant advantages in activating methanogenic process and augmented
564 performance under ammonia stress.

565 In summary, diverse light colors facilitated the carbon compound acidification in
566 different manners, yielding ample precursors for various methanogenic pathways.
567 Particularly, mix-color lighting robustly triggered enzymes that were pivotal for VFAs
568 degradation, and thus assisted to mitigate acid accumulation in ammonia-stressed AD.
569 Additionally, the light-enriched *Methanosarcina*, adept at utilizing triple substrates
570 (acetate, H_2/CO_2 and methanol), showed their power in Methane metabolism. Blue
571 and green lighting optimally stimulate key enzymes and cofactors across all
572 methanogenic pathways, while red lighting selectively activates the acetate-utilizing
573 *pta* enzyme. This underscored differential contributions of short and long wavelengths
574 within the visible light spectrum in regulating methanogenic activity, thereby leading
575 to a well-performed CH_4 conversion under ammonia stress.

576 **3.5.3 Energy conservation in light-assisted bionetwork**

577 Efficient organic conversion into CH_4 relies on the intricate syntrophic
578 cooperation and complex biochemical reactions among bacterial and archaeal
579 communities, which are driven by intracellular energy (ATP) and e^-. Energy yield is

commonly derived from the substrate phosphorylation and oxidative phosphorylation [70]. The core ATP-producing pathway, Oxidative phosphorylation, relies on the transmembrane gradient of Na^+/H^+ and e^- transfer, catalyzing the conversion of ADP to ATP through ATPase [B]. Genes involved in Oxidative phosphorylation showed higher abundance in Dark group compared to the lighted groups (Fig. 5), implying that the ammonia-stressed microbes in darkness required more energy in sustaining biochemical productivity than light-assisted anaerobes. In order to prove the hypothesis, gene abundances of the key enzymes involved in respiratory chain, including Complex Ⅰ (NADH: quinone oxidoreductase), Complex Ⅱ (succinate dehydrogenase), Complex Ⅲ (cytochrome bc1 complex) and Complex Ⅳ (cytochrome c oxidase) and ATPase (F-type and V/A type) were analyzed. As shown in Fig. 7a, e^- generated from substrate uptake is transferred to NAD^+ to produce NADH, which then diffuses to the cytoplasmic membrane and transports e^- to complex I. As e^- travels through the complex Ⅰ to Ⅳ, H^+ simultaneously transfers across the membrane, forming a proton motive force for ATP synthesis. Typically, bacteria primarily express genes encoding F-type ATPase for ATP synthesis, while V/A-type ATPase is employed by both bacteria and archaea to hydrolyze ATP and harness energy [71]. Compared to Dark group, lower gene expression coding for complex Ⅰ−Ⅳ and F-type ATPase (ATP synthase) was observed under single-color lighting (Fig. 7b), indicating less ATP generation via oxidative phosphorylation under monochromatic light stimulation. Instead, more energy may be yielded via substrate phosphorylation (e.g. light up-regulated glycolysis), given that 1 mol of glucose phosphorylation yields 2

602 ATP molecules (Table 2) [72]. Additionally, it has been reported that ATP synthesis is
603 associated with Energy-converting hydrogenase (Ech), acting as precursors to
604 Complex I [73]. Ech fuels H_2 production by utilizing the reduced ferredoxin (Fd_{rex}) as
605 e^- donor and coupling with NADH to reduce H^+, and the resulting H^+ force favors ATP
606 generation [33]. Compared to Dark group, a 48% elevation in Ech-coding gene
607 abundance was observed in the Blue and Green groups (Fig. 7c), suggesting an Ech-
608 mediated energy conservation occurred under short-wavelength lighting. Besides, the
609 generated H_2 could diffuse via IHT and participate in HM. Thus, short wavelengths
610 lighting might assist H_2 metabolism, preserving energy for cell anabolism under
611 ammonia stress.

612 Comparatively, the Mix group displayed relatively higher gene abundances
613 coding for Complex Ⅲ and Ⅳ (Fig. 7b), with a notable c-type cytochrome (Cyt C)
614 upregulation (Fig. 7c). In anaerobic respiratory, Cyt C serves dual roles: transferring
615 intermembrane e^- from Complex III to terminal acceptors (e.g., intracellular nitrate
616 and sulfate) [74] or shuttling e^- to extracellular acceptors (e.g., electroactive
617 methanogens) via IET [54]. According to Table 2, the syntrophic oxidation of VFAs
618 (propionate, butyrate and lactate) facilitated by IET was more thermodynamically
619 favorable ($\Delta G_0' < 0$) than that via traditional IHT (utilize H_2 as the e^- carrier).
620 Consequently, the Mix group exhibited lower gene expression encoding for V/A type-
621 ATPase (Fig. 7b), which hydrolyzes ATP and utilizes the released energy for energy-
622 dependent biochemical processes. The less energy demand in the Mix group might be
623 associated with the potentially formed IET pathway, in which the coenzyme F_{420} in

electroactive methanogens could directly accept the extracellular e^- and H^+ from acid-producing bacteria via Cyt C [74]. In contrast, the conventional IHT pathway for CH_4 production relies on a series of endergonic reactions to oxidize H_2/reduce CO_2 [68]. Thus, the bionetwork (acid degraders and methanogens) under mix-color light followed an energy-conserving metabolic pathway (Fig. 7a): the enriched syntrophic bacteria could harness the surplus e^- that generated from complex Ⅲ and Ⅳ (respiratory chain) and VFAs oxidation, transferring them to electroactive methanogens (*Methanosarcina* and *Methanoseata*) via energy-efficient association using Cyt C. This enhanced energy conservation and intercellular electronic cooperation potentially alleviated the metabolic imbalance between acid-producing bacteria and methanogens, addressing the VFAs accumulation in ammonia-inhibited AD. Moreover, the substantially upregulated QS for community association, cross-membrane transport and signal transduction in the Mix group (Fig. 5) also signified the activated extracellular metabolites export and communication within light-stimulated microflora. This aligned with prior studies reported that the incandescent light (400–800 nm) could elevate biomass activity [16,19], promote sludge conductivity [17] and favor the sludge colonization [20]. Moreover, the overexpressed Cyt C might also channel e^- to other energy-dependent pathways. For example, the other processes in energy metabolism (Nitrogen and Sulfur metabolism) were up-regulated under mix-color lighting (Fig. 5). This suggested that visible light stimulation had more advantages on optimizing the energy utilization in anaerobic community, which is fundamental for ensuring the active cell proliferation and

bioconversion efficiency during ammonia-stressed AD.

In summary, light regulated energy metabolism and syntrophic cooperation in a more energy-conserving way. Blue and green light stimulated the Ech activity, coupling the H_2 metabolism for energy generation, and subsequently favored the H_2-utilizing methanogenesis. Comparatively, mix-color lighting triggered the cross-membrane e^-generation with upregulated Cty C level, enhancing collaboration between e^- donating and accepting anaerobes. Therefore, mix-color lighting shifted the cell-cell collaboration towards exergonic IET under ammonia stress, saving more energy and redox equivalents for methanogenesis.

3.6 Proposed mechanism of light-triggered metabolic enhancement

By establishing connections among microbial structure, metabolic pathways, cell-cell interactions and digestion performance, the roles of light in different wavelengths were elucidated. Under single-color lighting, microbial abundance and diversity shared the similarity with the Dark group (Fig. 4b−e), characterized by lower levels of syntrophic VFAs oxidizers (Fig. 3a). However, relatively abundant sugar degraders, acidogenic bacteria, SAOB, and *Methanosarcina* contributed to improved performance under single-color lighting (Fig. 3b and Fig. 4a). Notably, light colors also exerted varying effects on metabolism. Glycolysis, Energy metabolism (e.g., sulfur and nitrogen metabolism), and Genetic information processing (e.g., Transcription and DNA replication) were influenced by blue and green light (Fig. 8a). Particularly, gene encoding key enzymes involved in AM, HM and MM were stimulated by blue and green lighting. These could be the main reasons for the similar

community with dark control, but better digestion performance observed in the Blue and Green groups. Whereas anaerobes in the Red group equipped with upregulated Two-component system, could directly sense red light signals and excite the cell cycle and motility (Fig. 8b). Consequently, red-light activated bacteria gained advantages in biomass growth and substrate uptake, facilitating rapid adaptation in shorten lag time (Fig. 1a) and accelerated acetate utilization (Fig. 2a).

While versatile *Methanosarcina* dominated in all the illuminated groups, the prevalences of HM (42–45%, calculated based on Fig. S3) were observed under single-color lighting. However, in the Mix group, both *Methanosarcina* and *Methanosaeta* experienced a maximal enrichment (Fig. 4a), and AM (42%) became the dominant methanogenic pathway (Fig. 8c). Mix-color lighting evenly enriched the diverse fermentative bacteria functioning in ammonia assimilation, sugar fermentation, VFAs degradation, and acetate oxidation (Fig. 3b). This could be attributed to the synergistic strengths of full wavelengths in mixed-color light, contributing not only to the enhanced microflora diversity, but also the activated cellular metabolism. Proposed mechanisms for mixed visible light-induced activation were outlined (Fig. 8c): (1) Microbes with different functions in the Mix group might catch the light signals (probably the long red waveband) via Signal transduction (Two-component system) on membrane firstly. (2) Light signals then might stimulate the cross-membrane transport system (PTS, bacterial secretion system), altering substrate uptake, carbohydrate metabolism, and metabolite export. (3) Membrane-associated respiratory chain units for e^- transport (complexes III, IV, and Cyt C) and energy

690 generation (ATPase) were regulated, leading to conservation of redox equivalents (e^-)
691 and energy (ATP) for cellular activity. (4) Excess e^- generated cross the membrane
692 could engage in intracellular ATP-dependent metabolisms (Nitrogen and Sulfur
693 metabolism) or participate in extracellular electronic flux through Cyt C. (5)
694 Sufficient Cyt C could channel e^- to electroactive methanogens in close proximity,
695 favoring IET-associated methanogenesis. (6) The electroactive methanogens
696 (*Methanosaeta* and *Methanosarcina*) directly utilized the extracellular redox
697 equivalents in respiration and Methane metabolism, which was particularly stimulated
698 by blue and green light (short wavelengths). (7) The IET-facilitated electronic
699 connections might enhance community-level QS systems, bolster cell-cell networks
700 and aggregation for synergistic organic conversion. Unlike the single-color lighting,
701 mix-color lighting could modulate the microbial behaviors at both the cell and
702 population levels, diversify the functional microbes and thus strengthen the
703 bioconversion of glucose → VFAs → acetate → CH_4 under ammonia stress.

704 **3.7 Novelty and implications**

705 Although employing light stimulation to enhance AD performance has gained
706 attention, the underlying mechanisms governing photoactivation within anaerobic
707 consortia remain largely unexplored. This study presented a novel focus on analyzing
708 the effects of light quality (light wavelengths) on ammonia-stressed AD from
709 comprehensive perspectives. Key findings included: (1) Irrespective of the light
710 wavelength, the dominance of *Methanosarcina* within the archaeal community
711 indicated an unprecedented affinity of these methanogens to light stimulation under

712 ammonia stress. (2) Light-enriched *Methanosarcina* behaved differently when
713 exposed to diverse wavelengths. Under single-color lighting, they were metabolically
714 active via CO_2 reduction pathway with an IHT-associated syntrophic bacteria
715 community. This H_2-dependent methanogenesis was highly associated with the
716 upregulated Ech and enzymes involved in HM under blue and green light, and the
717 enriched syntrophic SAOB under red light. However, when exposed to mixed visible
718 light, *Methanosarcina* preferred the acetate decarboxylation pathway for CH_4
719 conversion, which was facilitated by a more energy-efficient syntrophic network via
720 IET. Consequently, the growth and metabolism of anaerobes via electronic
721 collaboration were faster and more robust than conventional IHT, contributing to the
722 steadily increased CH_4 production and complete organic conversion under mixed
723 visible lighting. Notably, this study stands as the first to elucidate light-triggered
724 improvement by linking the gene abundance involved in cellular-level metabolism
725 with population-wide cell-cell networks. These novel discoveries could bridge the gap
726 to reveal the mystery of visible light stimulation on anaerobic bioprocess and guide
727 the practical transformation from lab scale to engineering scale.

728 From a long-term energy recovery and stability perspective, harnessing natural
729 visible light is a more environmentally friendly alternative to artificial LED lighting.
730 According to a 2-month semi-continuous study (Fig. S4), solar lighting within visible
731 wavelengths (370–800 nm) outperformed conventional dark AD across varying
732 ammonia inhibition levels (2500–5000 mg/L). This outcome underscored the
733 practical viability of establishing a solar-assisted bioconversion system for waste

734 treatment and renewable energy generation. In this system, no additional chemicals or
735 complex processes are required. And the input ammonia-rich feedstock (e.g., livestock
736 waste, blackwater and waste sludge) could be efficiently converted by naturally
737 derived anaerobes into clean, carbon-neutral biogas under sunlight. Furthermore,
738 bioinformatic analysis on microbial communities and metagenomic predictions
739 suggested that specific metabolic byproducts (e.g., raw H_2 and commercial VFAs) can
740 be generated by filtering specific wavelengths during fermentation. Consequently, the
741 scientific novelty coupled with practical implications of solar-assisted system
742 proposed by this study may pave the path for the future development of economically
743 feasible and environmentally friendly waste-to-energy system on a large scale.

744 **4. Conclusion**

745 This study pioneered a comprehensive exploration on the role of visible light
746 with different wavelengths in enhancing the ammonia-stressed anaerobic digestion.
747 Intricate relationships between light wavelengths and anaerobic consortium responses
748 were revealed based on the linkage among digestion performance, microbial structure
749 and metagenetic prediction. Short wavebands in blue and green light excited genes
750 encoding Energy metabolism and Methane metabolism, while long wavebands in red
751 light upregulated the Cell growth and Cell motility. Benefiting from the combined
752 strengths of short and long wavelengths, mix-color lighting outperformed the
753 digestion efficiency by forming a *Methanosarcina*-dominant microflora (90% of
754 methanogenic community) with optimal CH_4 generation pathways. The specifically
755 upregulated syntrophic acid oxidizing bacteria, electroactive methanogens and

extracellular electron transport system (c-type cytochrome and Quorum sensing) facilitated the cell-cell associations for fast and stable organic conversion into CH_4 under mixed visible light. This novel insight highlighted the potential of harnessing natural visible light to assist the organic bioconversion in practice, presenting a promising approach for ammonia-rich waste treatment and renewable energy production. This research collectively bridges knowledge gaps, providing insights into the profound influence of visible light on anaerobic bioprocesses, and offers a practical path toward sustainable waste-to-energy management in practical commercialization.

Acknowledgement

This research was supported by Scientific Research (B) 22H03778 and Grant-in-Aid for Exploratory Research 21k19628 from Japan Society for the Promotion of Science.

References

[1] H.Y. Leong, C.K. Chang, K.S. Khoo, K.W. Chew, S.R. Chia, J.W. Lim, J.S. Chang, P.L. Show, Waste biorefinery towards a sustainable circular bioeconomy: a solution to global issues, Biotechnol. Biofuels. 14 (2021) 1–15. https://doi.org/10.1186/s13068-021-01939-5.

[2] R. Ochieng, A. Gebremedhin, S. Sarker, Integration of Waste to Bioenergy Conversion Systems: A Critical Review, Energies. 15 (2022). https://doi.org/10.3390/en15072697.

[3] R. Bedoić, L. Čuček, B. Ćosić, D. Krajnc, G. Smoljanić, Z. Kravanja, D.

778 Ljubas, T. Pukšec, N. Duić, Green biomass to biogas – A study on anaerobic
779 digestion of residue grass, J. Clean. Prod. 213 (2019) 700–709.
780 https://doi.org/10.1016/J.JCLEPRO.2018.12.224.
781 [4] G. Li, F. Xu, T. Yang, X. Wang, T. Lyu, Z. Huang, Microbial Behavior and
782 Influencing Factors in the Anaerobic Digestion of Distiller: A Comprehensive
783 Review, Fermentation. 9 (2023) 1–29.
784 https://doi.org/10.3390/fermentation9030199.
785 [5] J. Liu, J. Luo, J. Zhou, Q. Liu, G. Qian, Z.P. Xu, Inhibitory effect of high-
786 strength ammonia nitrogen on bio-treatment of landfill leachate using EGSB
787 reactor under mesophilic and atmospheric conditions, Bioresour. Technol. 113
788 (2012) 239–243. https://doi.org/10.1016/j.biortech.2011.11.114.
789 [6] M. Czatzkowska, M. Harnisz, E. Korzeniewska, I. Koniuszewska, Inhibitors of
790 the methane fermentation process with particular emphasis on the
791 microbiological aspect: A review, Energy Sci. Eng. 8 (2020) 1880–1897.
792 https://doi.org/10.1002/ese3.609.
793 [7] S. Sawayama, K. Tsukara, T. Yagishita, Water treatment, Poly-b-
794 hydroxybutyrate production using lighted upflow anaerobic sludge blanket
795 method, J. Biosci. Bioeng. 87 (1999) 683–689.
796 [8] S. Sawayama, K. Tsukahara, T. Yagishita, S. Hanada, Characterization of
797 lighted upflow anaerobic sludge blanket (LUASB) method under sulfate-rich
798 conditions, J. Biosci. Bioeng. 91 (2001) 195–201.
799 https://doi.org/10.1016/S1389-1723(01)80065-7.

[9] C. Tada, S. Sawayama, Photoenhancement of biogas production from thermophilic anaerobic digestion, J. Biosci. Bioeng. 98 (2004) 387–390. https://doi.org/10.1016/s1389-1723(04)00301-9.

[10] C. Tada, K. Tsukahara, S. Sawayama, Illumination enhances methane production from thermophilic anaerobic digestion, Appl. Microbiol. Biotechnol. 71 (2006) 363–368. https://doi.org/10.1007/s00253-005-0146-z.

[11] A. Kiener, R. Gall, T. Rechsteiner, T. Leisinger, Photoreactivation in Methanobacterium thermoautotrophicum, Arch. Microbiol. 143 (1985) 147–150. https://doi.org/10.1007/BF00411038.

[12] K.D. Olson, C.W. Mcmahon, R.S. Wolfe, Photoactivation of the 2-(methylthio)ethanesulfonic acid reductase from Methanobacterium, Proc. Natl. Acad. Sci. U. S. A. (1991). https://doi.org/10.1073/pnas.88.10.4099.

[13] Y. Yang, K. Tsukahara, Z. Zhang, N. Sugiura, S. Sawayama, Optimization of illumination time for the production of methane using carbon felt fluidized bed bioreactor in thermophilic anaerobic digestion, Biochem. Eng. J. 44 (2009) 131–135. https://doi.org/10.1016/j.bej.2008.11.009.

[14] Y. Yang, K. Tsukahara, R. Yang, Z. Zhang, S. Sawayama, Enhancement on biodegradation and anaerobic digestion efficiency of activated sludge using a dual irradiation process, Bioresour. Technol. 102 (2011) 10767–10771. https://doi.org/10.1016/j.biortech.2011.09.018.

[15] M.S. Majeed, R.Q. Nafil, R.K. Fakher Alfahed, Laser improves biogas production by anaerobic digestion of cow dung, Baghdad Sci. J. 15 (2018)

822 324–327. https://doi.org/10.21123/bsj.2018.15.3.0324.
823 [16] N. Zhang, M.S. Stanislaus, X. Hu, C. Zhao, Q. Zhu, D. Li, Y. Yang, Strategy of
824 mitigating ammonium-rich waste inhibition on anaerobic digestion by using
825 illuminated bio-zeolite fixed-bed process, Bioresour. Technol. 222 (2016) 59–
826 65. https://doi.org/10.1016/j.biortech.2016.09.053.
827 [17] H. Zheng, A. Sharma, Q. Ma, C. Zhang, T. Hiranuma, Y. Chen, G. Chen, Y.
828 Yang, Development of an oyster shell and lignite modified zeolite (OLMZ)
829 fixed bioreactor coupled with intermittent light stimulation for high efficient
830 ammonium-rich anaerobic digestion process, Chem. Eng. J. 398 (2020) 161.
831 https://doi.org/10.1016/j.cej.2020.125637.
832 [18] Y. Zhu, N. Zhang, Z. Liu, N. Liu, A. Sharma, G. Chen, Y. Yang, Photon
833 number based anaerobic digestion process for efficient bio-methane conversion
834 from ammonium-rich feedstock: Performance evaluation and practical potential,
835 Energy Convers. Manag. 238 (2021) 114155.
836 https://doi.org/10.1016/J.ENCONMAN.2021.114155.
837 [19] Z. Liu, Y. Zhu, C. Zhao, C. Zhang, J. Ming, A. Sharma, G. Chen, Y. Yang,
838 Light stimulation strategy for promoting bio-hydrogen production: Microbial
839 community, metabolic pathway and long-term application, Bioresour. Technol.
840 350 (2022) 126902. https://doi.org/10.1016/j.biortech.2022.126902.
841 [20] Y. Zhu, Z. Liu, C. Zhang, J. Ming, G. Chen, Y. Yang, Light triggers green
842 recovery: Boosted biomethane production from ammonia-stressed anaerobic
843 digestion through optimized illuminated bioreactor, Chem. Eng. J. 450 (2022)

138173. https://doi.org/10.1016/j.cej.2022.138173.

[21] J. Qian, Y. Zhang, P. Wang, B. Lu, Y. He, S. Tang, Z. Yi, Light alters microbiota and electron transport: Evidence for enhanced mesophilic digestion of municipal sludge, Water Res. 217 (2022) 118447. https://doi.org/10.1016/j.watres.2022.118447.

[22] P. Sowa, J. Rutkowska-Talipska, K. Rutkowski, B. Kosztyła-Hojna, R. Rutkowski, Optical radiation in modern medicine, Postep. Dermatologii i Alergol. 30 (2013) 246–251. https://doi.org/10.5114/pdia.2013.37035.

[23] T. Karu, L. Pyatibrat, G. Kalendo, Irradiation with He-Ne laser increases ATP level in cells cultivated in vitro, J. Photochem. Photobiol. B Biol. 27 (1995) 219–223.

[24] T.J. Karu, O.A. Tiphlova, V.S. Letokhov, V. V. Lobko, Stimulation of E. coli growth by laser and incoherent red light, Nuovo Cim. D 1983 24. 2 (1983) 1138–1144. https://doi.org/10.1007/BF02457148.

[25] K.D. Olson, C.W. McMahon, R.S. Wolfe, Light sensitivity of methanogenic archaebacteria, Appl. Environ. Microbiol. 57 (1991) 2683–2686. https://doi.org/https://doi.org/10.1128/aem.57.9.2683-2686.1991.

[26] E.J. Lyon, S. Shima, G. Buurman, S. Chowdhuri, A. Batschauer, K. Steinbach, R.K. Thauer, UV-A/blue-light inactivation of the “metal-free” hydrogenase (Hmd) from methanogenic archaea: The enzyme contains functional iron after all, Eur. J. Biochem. 271 (2004) 195–204. https://doi.org/10.1046/j.1432-1033.2003.03920.x.

[27] J. Zhang, L. Mao, L. Zhang, K.C. Loh, Y. Dai, Y.W. Tong, Metagenomic insight into the microbial networks and metabolic mechanism in anaerobic digesters for food waste by incorporating activated carbon, Sci. Rep. 7 (2017) 11293. https://doi.org/10.1038/s41598-017-11826-5.

[28] S. Yang, Z. Chen, Q. Wen, Impacts of biochar on anaerobic digestion of swine manure: Methanogenesis and antibiotic resistance genes dissemination, Bioresour. Technol. 324 (2021) 124679. https://doi.org/10.1016/J.BIORTECH.2021.124679.

[29] S.H. Yoon, S.M. Ha, S. Kwon, J. Lim, Y. Kim, H. Seo, J. Chun, Introducing EzBioCloud: A taxonomically united database of 16S rRNA gene sequences and whole-genome assemblies, Int. J. Syst. Evol. Microbiol. 67 (2017) 1613–1617. https://doi.org/10.1099/ijsem.0.001755.

[30] S. Poirier, C. Madigou, T. Bouchez, O. Chapleur, Improving anaerobic digestion with support media: Mitigation of ammonia inhibition and effect on microbial communities, Bioresour. Technol. 235 (2017) 229–239. https://doi.org/10.1016/j.biortech.2017.03.099.

[31] S. Passarella, E. Casamassima, S. Molinari, D. Pastore, E. Quagliariello, I.M. Catalano, A. Cingolani, Increase of proton electrochemical potential and ATP synthesis in rat liver mitochondria irradiated in vitro by helium-neon laser, FEBS Lett. 175 (1984) 95–99. https://doi.org/10.1016/0014-5793(84)80577-3.

[32] E. Abdelsalam, M. Samer, M.A. Abdel-Hadi, H.E. Hassan, Y. Badr, Influence of laser irradiation on rumen fluid for biogas production from dairy manure,

888 Energy. 163 (2018) 404–415. https://doi.org/10.1016/J.ENERGY.2018.08.118.
889 [33] X. Pan, L. Zhao, C. Li, I. Angelidaki, N. Lv, J. Ning, G. Cai, G. Zhu, Deep
890 insights into the network of acetate metabolism in anaerobic digestion:
891 focusing on syntrophic acetate oxidation and homoacetogenesis, Water Res.
892 190 (2021) 116774. https://doi.org/10.1016/j.watres.2020.116774.
893 [34] M. Felchner-Zwirello, Propionic acid degradation by syntrophic bacteria during
894 anaerobic biowaste digestion, 2014. https://doi.org/10.5445/KSP/1000037825.
895 [35] S. Poirier, E. Desmond-Le Quéméner, C. Madigou, T. Bouchez, O. Chapleur,
896 Anaerobic digestion of biowaste under extreme ammonia concentration:
897 Identification of key microbial phylotypes, Bioresour. Technol. 207 (2016) 92–
898 101. https://doi.org/10.1016/J.BIORTECH.2016.01.124.
899 [36] M. Yan, L. Treu, S. Campanaro, H. Tian, X. Zhu, B. Khoshnevisan, P.
900 Tsapekos, I. Angelidaki, I.A. Fotidis, Effect of ammonia on anaerobic digestion
901 of municipal solid waste: Inhibitory performance, bioaugmentation and
902 microbiome functional reconstruction, Chem. Eng. J. 401 (2020).
903 https://doi.org/10.1016/j.cej.2020.126159.
904 [37] Y. Yan, M. Yan, G. Ravenni, I. Angelidaki, D. Fu, I.A. Fotidis, Novel
905 bioaugmentation strategy boosted with biochar to alleviate ammonia toxicity in
906 continuous biomethanation, Bioresour. Technol. 343 (2022) 126146.
907 https://doi.org/10.1016/J.BIORTECH.2021.126146.
908 [38] X. Wang, P. Wang, X. Meng, L. Ren, Performance and metagenomics analysis
909 of anaerobic digestion of food waste with adding biochar supported nano zero-

910 valent iron under mesophilic and thermophilic condition, Sci. Total Environ.
911 820 (2022) 153244. https://doi.org/10.1016/j.scitotenv.2022.153244.
912 [39] S. Esquivel-Elizondo, P. Parameswaran, A.G. Delgado, J. Maldonado, B.E.
913 Rittmann, R. Krajmalnik-Brown, Archaea and bacteria acclimate to high total
914 ammonia in a methanogenic reactor treating swine waste, Archaea. (2016)
915 4089684. https://doi.org/10.1155/2016/4089684.
916 [40] D. Ho, P. Jensen, M.L. Gutierrez-Zamora, S. Beckmann, M. Manefield, D.
917 Batstone, High-rate, high temperature acetotrophic methanogenesis governed
918 by a three population consortium in anaerobic bioreactors, PLoS One. 11 (2016)
919 e0159760. https://doi.org/10.1371/JOURNAL.PONE.0159760.
920 [41] Z. Wang, Y. Guo, W. Wang, L. Chen, Y. Sun, T. Xing, X. Kong, Effect of
921 biochar addition on the microbial community and methane production in the
922 rapid degradation process of corn straw, Energies. 14 (2021) 2223.
923 https://doi.org/10.3390/en14082223.
924 [42] R. Arthur, S. Antonczyk, S. Off, P.A. Scherer, Mesophilic and thermophilic
925 anaerobic digestion of wheat straw in a CSTR system with ‘synthetic manure’:
926 impact of nickel and tungsten on methane yields, cell count, and microbiome,
927 Bioengineering. 9 (2022) 13. https://doi.org/10.3390/bioengineering9010013.
928 [43] A. Poehlein, V. V. Zverlov, R. Daniel, W.H. Schwarz, W. Liebl, Complete
929 genome sequence of Clostridium stercorarium subsp. stercorarium strain DSM
930 8532, a thermophilic degrader of plant cell wall fibers, Genome Announc. 1
931 (2013) 8–9. https://doi.org/10.1128/genomeA.00073-13.

[44] X. Dai, H. Yan, N. Li, J. He, Y. Ding, L. Dai, B. Dong, Metabolic adaptation of microbial communities to ammonium stress in a high solid anaerobic digester with dewatered sludge, Sci. Rep. 6 (2016) 1–10. https://doi.org/10.1038/srep28193.

[45] G. Lembo, S. Rosa, V.M. Miritana, A. Marone, G. Massini, M. Fenice, A. Signorini, Thermophilic anaerobic digestion of second cheese whey: microbial community response to H2 addition in a partially immobilized anaerobic hybrid reactor, Process. 2021, Vol. 9, Page 43. 9 (2020) 43. https://doi.org/10.3390/PR9010043.

[46] H. Tian, E. Mancini, L. Treu, I. Angelidaki, I.A. Fotidis, Bioaugmentation strategy for overcoming ammonia inhibition during biomethanation of a protein-rich substrate, Chemosphere. 231 (2019) 415–422. https://doi.org/10.1016/j.chemosphere.2019.05.140.

[47] C. Liu, Y. Chen, H. Huang, X. Duan, L. Dong, Improved anaerobic digestion under ammonia stress by regulating microbiome and enzyme to enhance VFAs bioconversion: The new role of glutathione, Chem. Eng. J. 433 (2022) 134562. https://doi.org/10.1016/J.CEJ.2022.134562.

[48] S. Wainaina, Lukitawesa, M. Kumar Awasthi, M.J. Taherzadeh, Bioengineering of anaerobic digestion for volatile fatty acids, hydrogen or methane production: A critical review, Bioengineered. 10 (2019) 437–458. https://doi.org/10.1080/21655979.2019.1673937.

[49] D.G. Zavarzina, T.P. Tourova, T. V. Kolganova, E.S. Boulygina, T.N. Zhilina,

954 Description of Anaerobacillus alkalilacustre gen. nov., sp. nov.—Strictly
955 anaerobic diazotrophic bacillus isolated from soda lake and transfer of Bacillus
956 arseniciselenatis, Bacillus macyae, and Bacillus alkalidiazotrophicus to
957 Anaerobacillus as the new combinations A. arseniciselenatis comb. nov., A.
958 macyae comb. nov., and A. alkalidiazotrophicus comb. nov., Microbiol. 2009
959 786. 78 (2009) 723–731. https://doi.org/10.1134/S0026261709060095.
960 [50] N. Ahsan, M. Shimizu, Lysinibacillus species: Their potential as effective
961 bioremediation, biostimulant, and biocontrol agents, Rev. Agric. Sci. 9 (2021)
962 103–116. https://doi.org/10.7831/RAS.9.0_103.
963 [51] H. Tian, I.A. Fotidis, E. Mancini, L. Treu, A. Mahdy, M. Ballesteros, C.
964 González-Fernández, I. Angelidaki, Acclimation to extremely high ammonia
965 levels in continuous biomethanation process and the associated microbial
966 community dynamics, Bioresour. Technol. 247 (2018) 616–623.
967 https://doi.org/10.1016/J.BIORTECH.2017.09.148.
968 [52] Q. Niu, T. Kobayashi, Y. Takemura, K. Kubota, Y.Y. Li, Evaluation of
969 functional microbial community's difference in full-scale and lab-scale
970 anaerobic digesters feeding with different organic solid waste: Effects of
971 substrate and operation factors, Bioresour. Technol. 193 (2015) 110–118.
972 https://doi.org/10.1016/j.biortech.2015.05.107.
973 [53] X. Zhu, S. Campanaro, L. Treu, R. Seshadri, N. Ivanova, P.G. Kougias, N.
974 Kyrpides, I. Angelidaki, Metabolic dependencies govern microbial syntrophies
975 during methanogenesis in an anaerobic digestion ecosystem, Microbiome. 8

(2020) 1–14. https://doi.org/10.1186/S40168-019-0780-9/FIGURES/6.

[54] L. Li, Y. Xu, X. Dai, L. Dai, Principles and advancements in improving anaerobic digestion of organic waste via direct interspecies electron transfer, Renew. Sustain. Energy Rev. 148 (2021) 111367. https://doi.org/10.1016/J.RSER.2021.111367.

[55] Y. Jiang, E. McAdam, Y. Zhang, S. Heaven, C. Banks, P. Longhurst, Ammonia inhibition and toxicity in anaerobic digestion: A critical review, J. Water Process Eng. 32 (2019). https://doi.org/10.1016/j.jwpe.2019.100899.

[56] T.L. Netzel, Electron transfer reactions in methanogens, J. Chem. Educ. 74 (1997) 646–651. https://doi.org/10.1021/ed074p646.

[57] B. Müller, L. Sun, M. Westerholm, A. Schnürer, Bacterial community composition and fhs profiles of low- and high-ammonia biogas digesters reveal novel syntrophic acetate-oxidising bacteria, Biotechnol. Biofuels. 9 (2016) 48. https://doi.org/10.1186/S13068-016-0454-9.

[58] S.J. Haig, C. Quince, R.L. Davies, C.C. Dorea, G. Collinsa, The relationship between microbial community evenness and function in slow sand filters, MBio. 6 (2015) e00729-15. https://doi.org/10.1128/mBio.00729-15.

[59] W. Zhang, X. Li, Y. He, X. Xu, H. Chen, A. Zhang, Y. Liu, G. Xue, J. Makinia, Ammonia amendment promotes high rate lactate production and recovery from semi-continuous food waste fermentation, Bioresour. Technol. 302 (2020) 122881. https://doi.org/10.1016/J.BIORTECH.2020.122881.

[60] T.R.D. Costa, C. Felisberto-Rodrigues, A. Meir, M.S. Prevost, A. Redzej, M.

998 Trokter, G. Waksman, Secretion systems in Gram-negative bacteria: structural
999 and mechanistic insights, Nat. Rev. Microbiol. 2015 136. 13 (2015) 343–359.
1000 https://doi.org/10.1038/nrmicro3456.
1001 [61] T. Zhang, P. Zhang, Z. Hu, Q. Qi, Y. He, J. Zhang, New insight on Fe-
1002 bioavailability: Bio-uptake, utilization and induce in optimizing methane
1003 production in anaerobic digestion, Chem. Eng. J. 441 (2022) 136099.
1004 https://doi.org/10.1016/J.CEJ.2022.136099.
1005 [62] M. Wang, X. Zhang, H. Huang, Z. Qin, C. Liu, Y. Chen, Amino Acid
1006 Configuration Affects Volatile Fatty Acid Production during Proteinaceous
1007 Waste Valorization: Chemotaxis, Quorum Sensing, and Metabolism, Cite This
1008 Environ. Sci. Technol. 2022 (2022) 8711.
1009 https://doi.org/10.1021/acs.est.1c07894.
1010 [63] L.L. Barton, Structural and Functional Relationships in Prokaryotes, Springer-
1011 Verlag, 2005. https://doi.org/10.1007/b138652.
1012 [64] Z. Zhao, J. Wang, Y. Li, T. Zhu, Q. Yu, T. Wang, S. Liang, Y. Zhang, Why do
1013 DIETers like drinking: Metagenomic analysis for methane and energy
1014 metabolism during anaerobic digestion with ethanol, Water Res. 171 (2020)
1015 115425. https://doi.org/10.1016/j.watres.2019.115425.
1016 [65] J. Cheng, H. Li, L. Ding, J. Zhou, W. Song, Y.Y. Li, R. Lin, Improving
1017 hydrogen and methane co-generation in cascading dark fermentation and
1018 anaerobic digestion: The effect of magnetite nanoparticles on microbial
1019 electron transfer and syntrophism, Chem. Eng. J. 397 (2020) 125394.

https://doi.org/10.1016/j.cej.2020.125394.

[66] N. Zhang, H. Peng, Y. Li, W. Yang, Y. Zou, H. Duan, Ammonia determines transcriptional profile of microorganisms in anaerobic digestion, Brazilian J. Microbiol. 49 (2018) 770–776. https://doi.org/10.1016/j.bjm.2018.04.008.

[67] S. Dyksma, L. Jansen, C. Gallert, Syntrophic acetate oxidation replaces acetoclastic methanogenesis during thermophilic digestion of biowaste, Microbiome. 8(1) (2020) 1–14. https://doi.org/10.1186/s40168-020-00862-5.

[68] C. Welte, U. Deppenmeier, Bioenergetics and anaerobic respiratory chains of aceticlastic methanogens, Biochim. Biophys. Acta - Bioenerg. 1837 (2014) 1130–1147. https://doi.org/10.1016/j.bbabio.2013.12.002.

[69] F. Mahlert, C. Bauer, B. Jaun, R.K. Thauer, E.C. Duin, The nickel enzyme methyl-coenzyme M reductase from methanogenic archaea: In vitro induction of the nickel-based MCR-ox EPR signals from MCR-red2, J. Biol. Inorg. Chem. 7 (2002) 500–513. https://doi.org/10.1007/s00775-001-0325-z.

[70] P. Mitchell and J. Moyle., Evidence discriminating between the Chemical and the Chemiosmotic Mechanisms of Electron Transport Phosphorylation, Nature. 208 (1965) 1205–1206. https://doi.org/https://doi.org/10.1038/2081205a0.

[71] L.J. Bird, V. Bonnefoy, D.K. Newman, Bioenergetic challenges of microbial iron metabolisms, Trends Microbiol. 19 (2011) 330–340. https://doi.org/10.1016/J.TIM.2011.05.001.

[72] S. Lenzen, A fresh view of glycolysis and glucokinase regulation: History and current status, J. Biol. Chem. 289 (2014) 12189–12194.

https://doi.org/10.1074/jbc.R114.557314.

[73] M.C. Schoelmerich, V. Müller, Energy-converting hydrogenases: the link between H2 metabolism and energy conservation, Cell. Mol. Life Sci. 77 (2020) 1461–1481. https://doi.org/10.1007/S00018-019-03329-5.

[74] M. Wang, T. Ren, M. Yin, K. Lu, H. Xu, X. Huang, X. Zhang, Enhanced Anaerobic Wastewater Treatment by a Binary Electroactive Material : Pseudocapacitance / Conductance-Mediated Microbial Interspecies Electron Transfer, (2023). https://doi.org/10.1021/acs.est.3c01986.

Table 1 Kinetic parameters of modified Gompertz model on lighted AD with different wavelengths

Parameter \ Group	Dark	Blue	Green	Red	Mix
Start up					
M_{max}	228	593	172	1014	797
R_{max}	86	253	415	292	91
λ	2.1	2.9	0.7	1.3	0.4
R^2	0.990	0.975	0.992	0.978	0.931
Cycle 1					
M_{max}	158	489	452	438	778
R_{max}	141	487	703	420	828
λ	0.6	0.3	0.2	0.1	0.5
R^2	0.990	0.993	0.999	0.974	0.999
Cycle 2					
M_{max}	254	123	489	546	628
R_{max}	122	60	523	656	690
λ	0.9	0.8	0.2	0.9	0.7
R^2	0.999	0.991	0.997	0.999	0.998

M_{max}: maximum cumulative methane production in each cycle, (mL/L)

R_{max}: maximum methane production rate, (mL/(L·d))

λ: lag-phase time, (d)

Table 2 Common reactions and thermodynamics of AD via interspecies hydrogen transfer (IHT) and interspecies electron transfer (IET) pathways.

	Pathway		Equation	ΔG_0' (kJ/mol)	Reference
	Glycolysis		$C_6H_{12}O_6 + 2NAD^+ + 2ADP + 2Pi \rightarrow 2C_3H_4O_3 + 2NADH + 2H^+ + 2ATP + 2H_2O$	− 96.0	[72]
Acidification	Syntrophic propionate oxidation	IHT	$C_3H_5OO^- + 2H_2O \rightarrow CH_3COO^- + 3H_2 + CO_2$	+ 76.5	[54]
		IET	$C_3H_5OO^- + 3H_2O \rightarrow CH_3COO^- + HCO_3^- + 7H^+ + 6e^-$	− 162.5	
	Syntrophic butyrate oxidation	IHT	$C_4H_7OO^- + 2H_2O \rightarrow 2CH_3COO^- + 2H_2 + H^+$	+ 48.0	
		IET	$C_4H_7OO^- + 2H_2O \rightarrow 2CH_3COO^- + 5H^+ + 4e^-$	− 111.3	
	Syntrophic lactate oxidation	IHT	$2C_3H_5O_3^- + 2H_2O \rightarrow 2CH_3COO^- + HCO_3^- + H^+ + 2H_2$	− 4.2	
		IET	$2C_3H_5O_3^- + 2H_2O \rightarrow CH_3COO^- + + HCO_3^- + 5H^+ + 4e^-$	− 163.5	
	Syntrophic acetate oxidation		$CH_3COO^- + 4H_2O \rightarrow 2HCO_3^- + 4H_2 + H^+$	+ 104.6	
Methanogenesis	Hydrogenotrophic		$4H_2 + HCO_3^- + H^+ \rightarrow CH_4 + 3H_2O$	− 131.0	[52]
	Acetoclastic		$CH_3COO^- + H_2O \rightarrow CH_4 + HCO_3^-$	− 36.0	
	Methylotrophic		$4CH_3OH \rightarrow 3CH_4 + HCO_3^- + H^+ + H_2O$	− 105.0	

Figure

Fig. 1. Effect of light wavelengths on ammonia-rich AD performance of **(a)** cumulative CH_4 production, and **(b)** daily CH_4 concentration during three-cycle feed batch (Error bars presented standard deviations of repeated experiments).

Fig. 2. Effect of light wavelengths on variations of organic byproducts of **(a)** acetate, and **(b)** lactate, butyrate and propionate during three-cycle during ammonia-rich AD (bars presented standard deviations of repeated experiments).

Fig. 3. Variation of bacterial community under dark and light treatments. **(a)** Relative abundance of bacterial community at order level; **(b)** heat map with cluster analysis of dominant bacterial genus under each treatment.

Fig. 4. (a) Relative abundance of archaeal community at species level under each treatment, and boxplots for microbial richness and diversity with indexes of **(b)** observed species, **(c)** Chao1, **(d)** phylogenetic diversity (PD) whole tree and **(e)** Shannon (The *** and ** show significant differences ($P < 0.05$) and relatively different ($0.05 < P < 0.1$), respectively).

Fig. 5. Heatmap of relative gene abundance coding for metabolic pathway at level 3 based on metagenomic analysis (the corresponded functional categories at level 2 were listed on the right y-axis).

Fig. 6. (a) Conceptual graph and marker enzymes involved AM, HM and MM pathways, and **(b)** Heat map of gene abundance coding for key enzymes involved in methanogenic pathways under dark and light treatments.

Fig. 7. (a) Conceptual graph of pathways related to Energy Metabolism in bacteria and archaea based on KEGG mapper, **(b)** relative abundance of genes coding for complex

units in respiratory chain for ATP production, and **(c)** relative abundance of energy-converting hydrogenase (Ech) and c-type cytochrome (Cyt C).

Fig. 8. Mechanisms of light-triggered metabolic enhancement with **(a)** short wavelength (blue and green light), **(b)** long wavelength **(**red light), and **(c)** mix-color visible light.

Figure

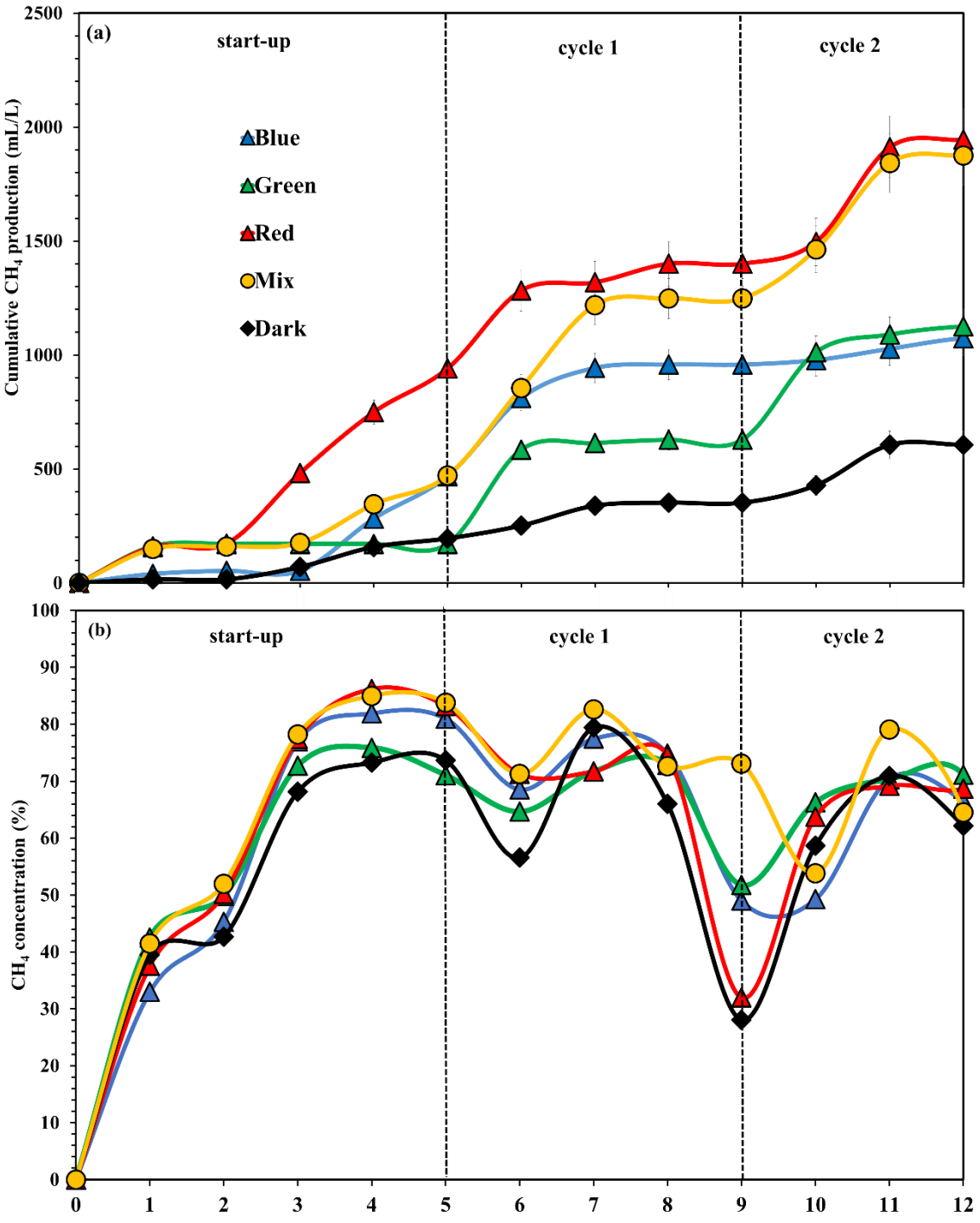

Figure 1

Figure

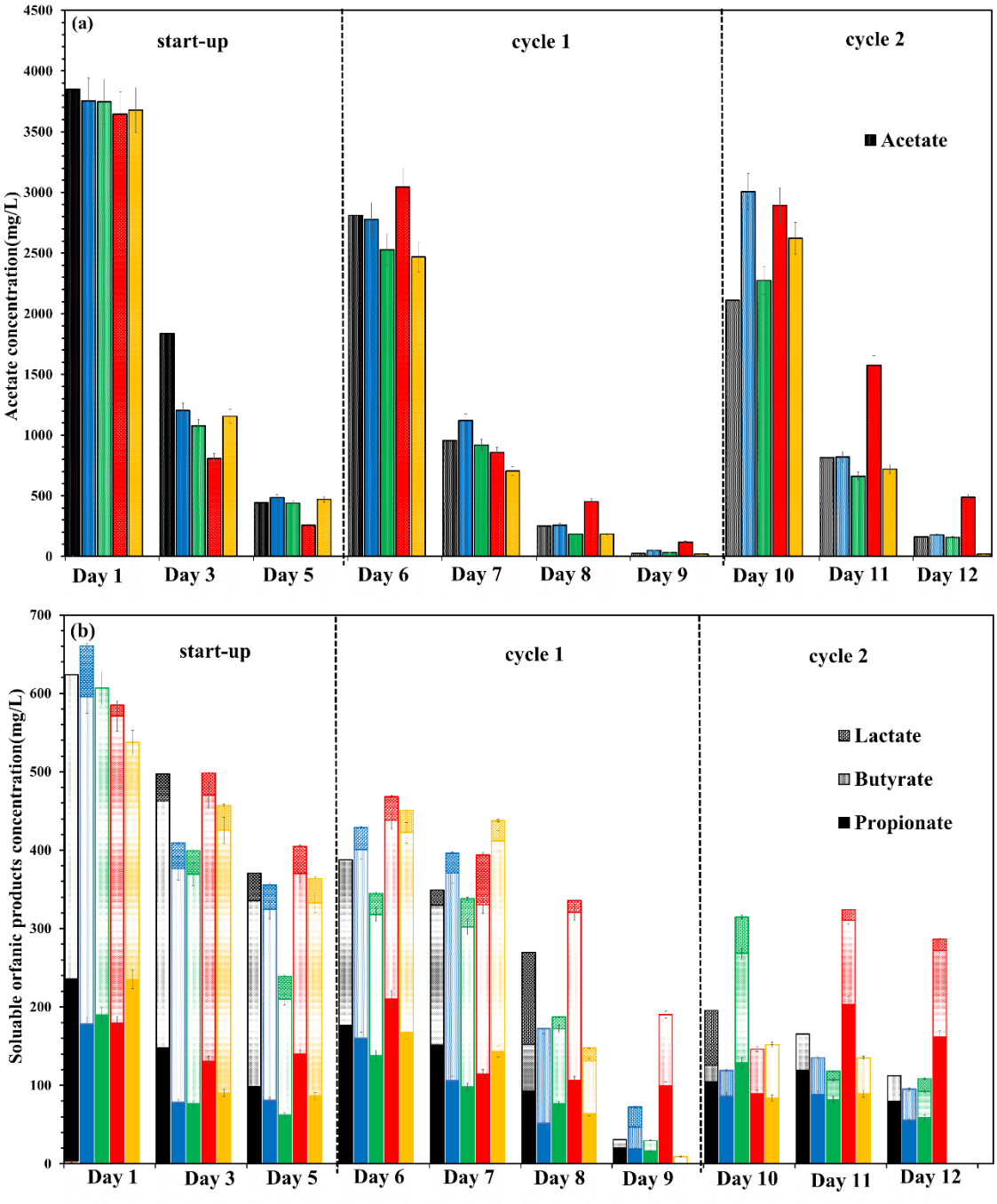

Figure 2

Figure

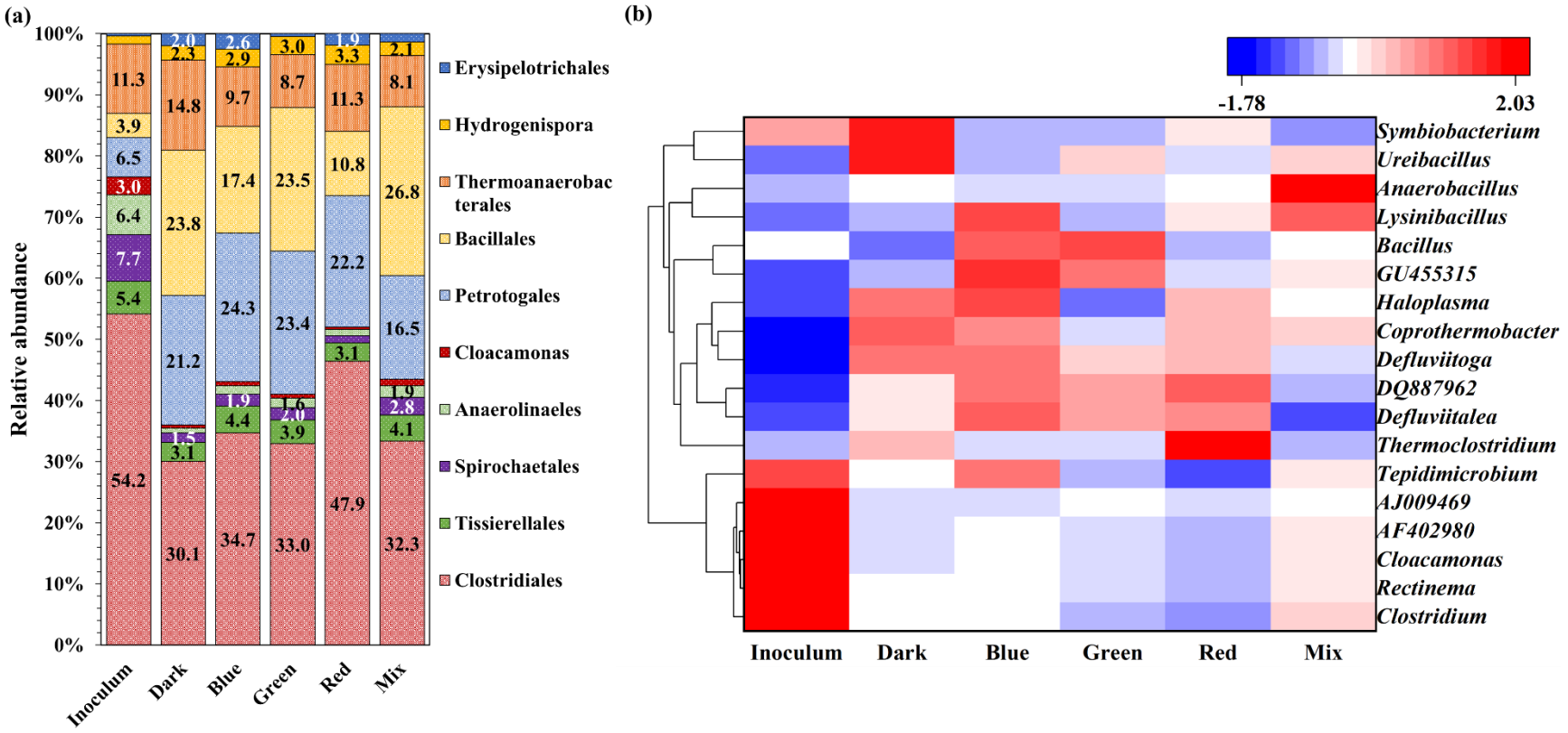

Figure 3

Figure

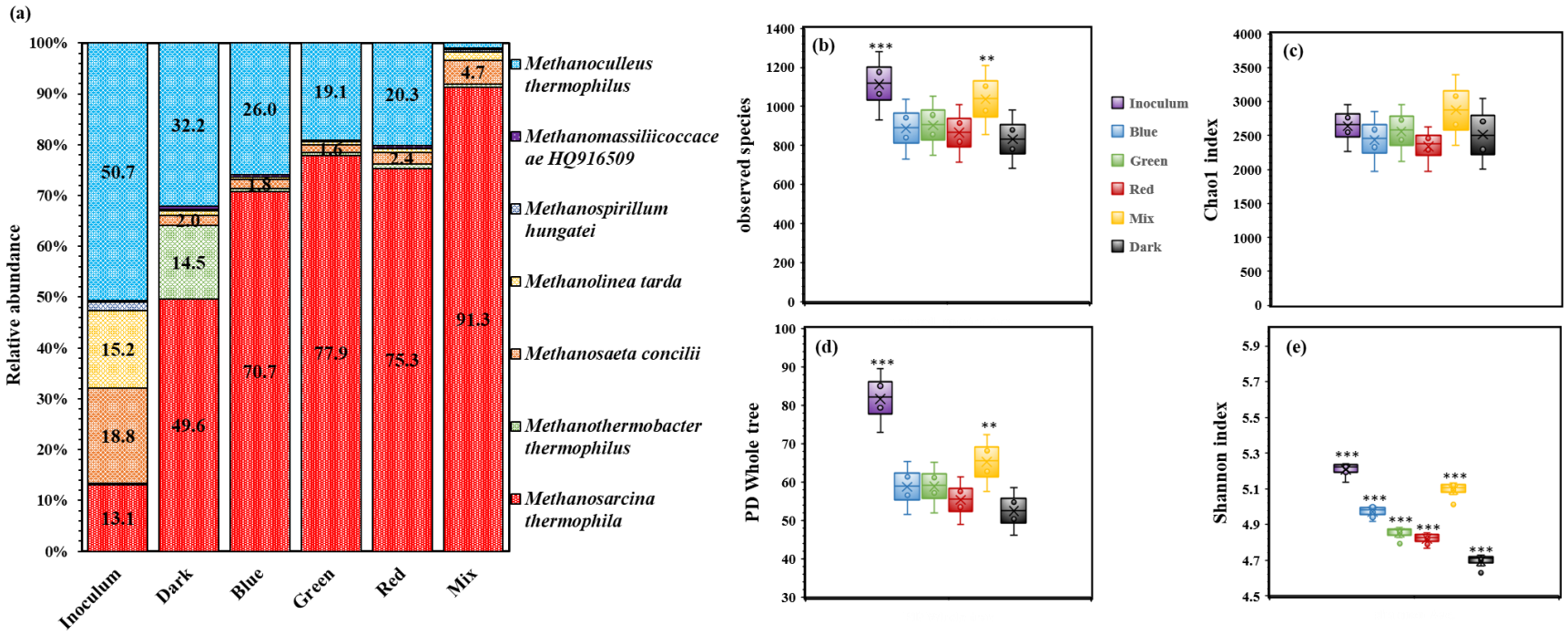

Figure 4

Figure

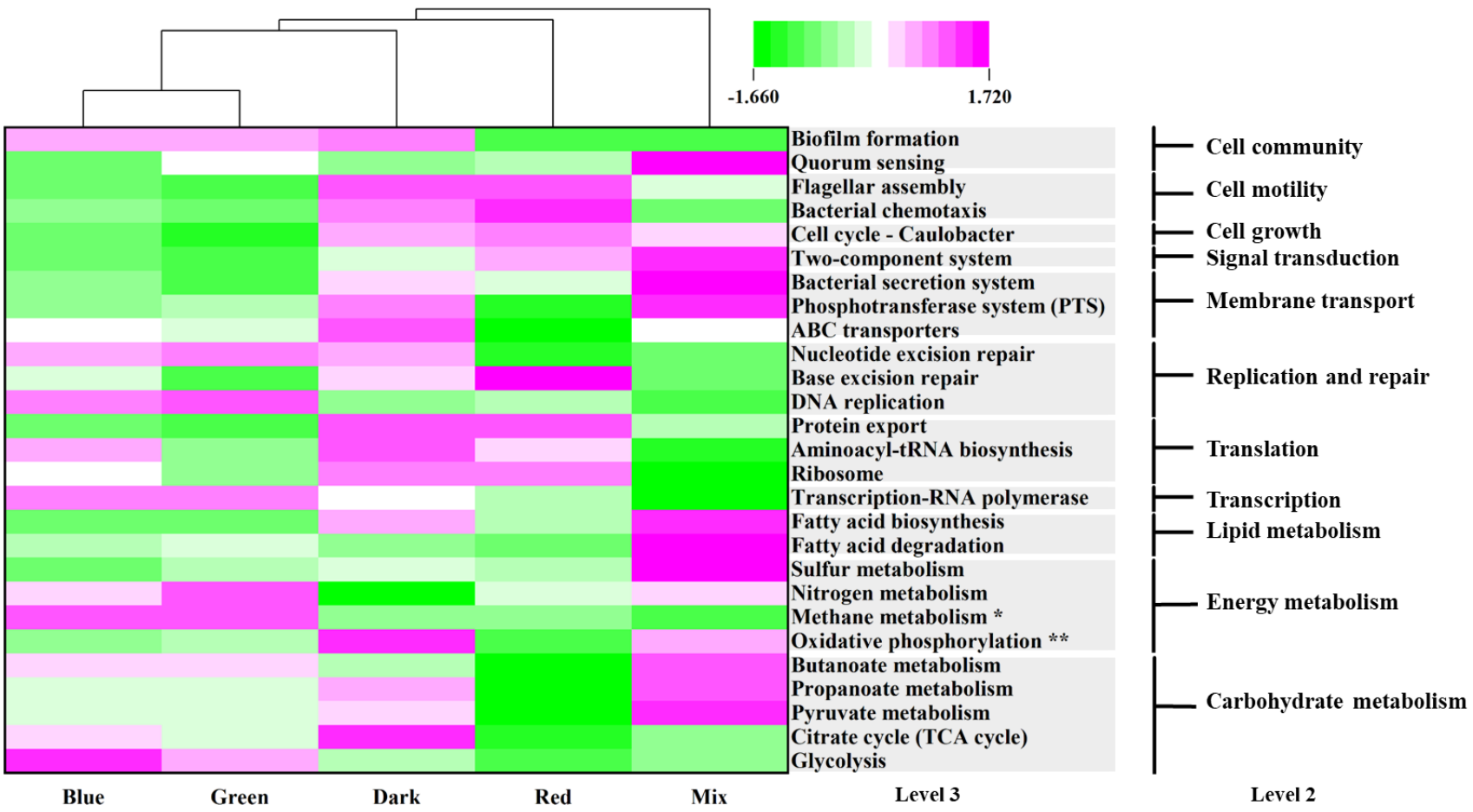

Figure 5

Figure

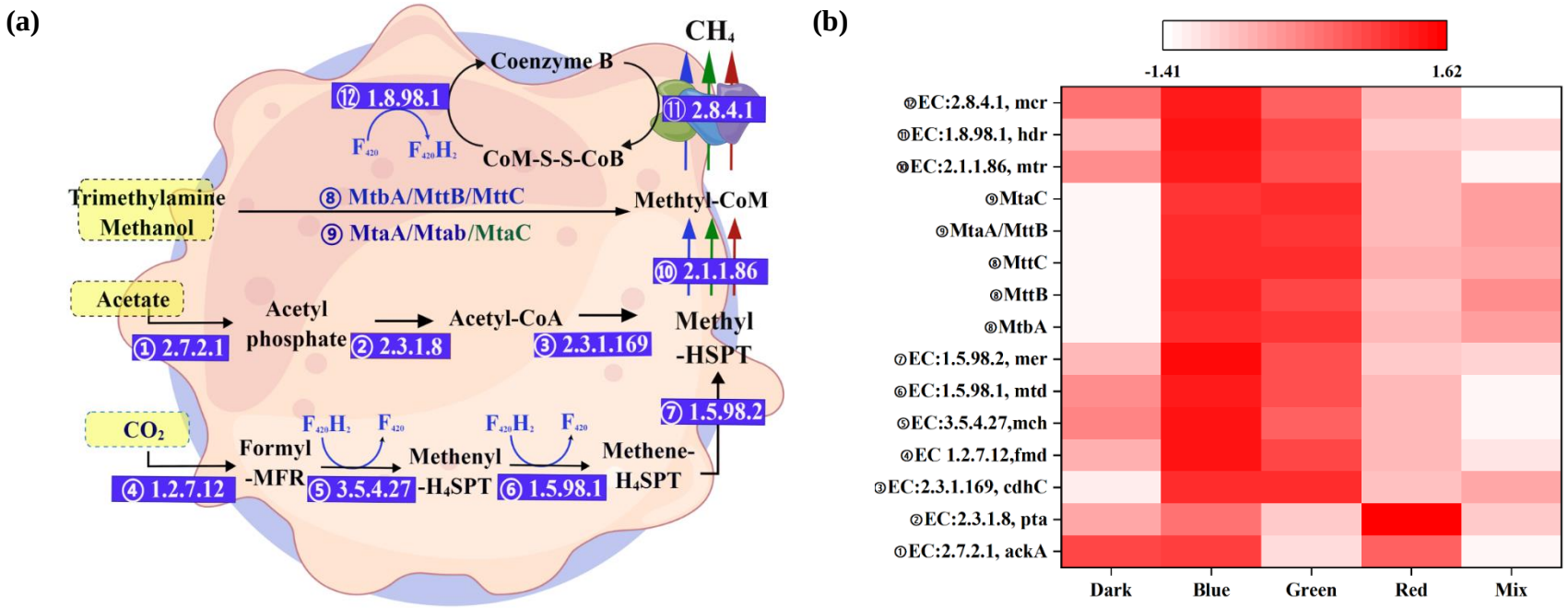

Figure 6

Figure

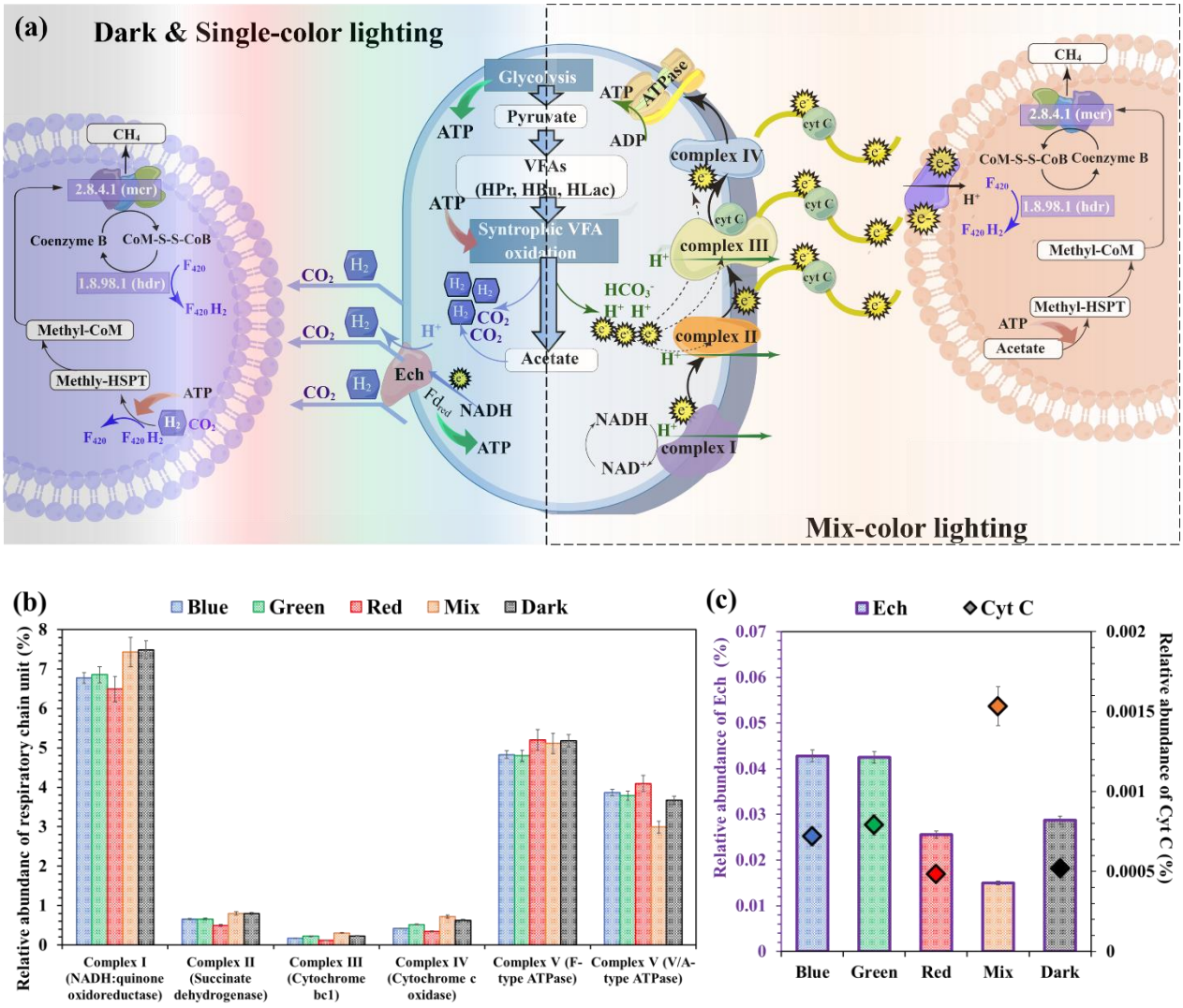

Figure 7

Figure

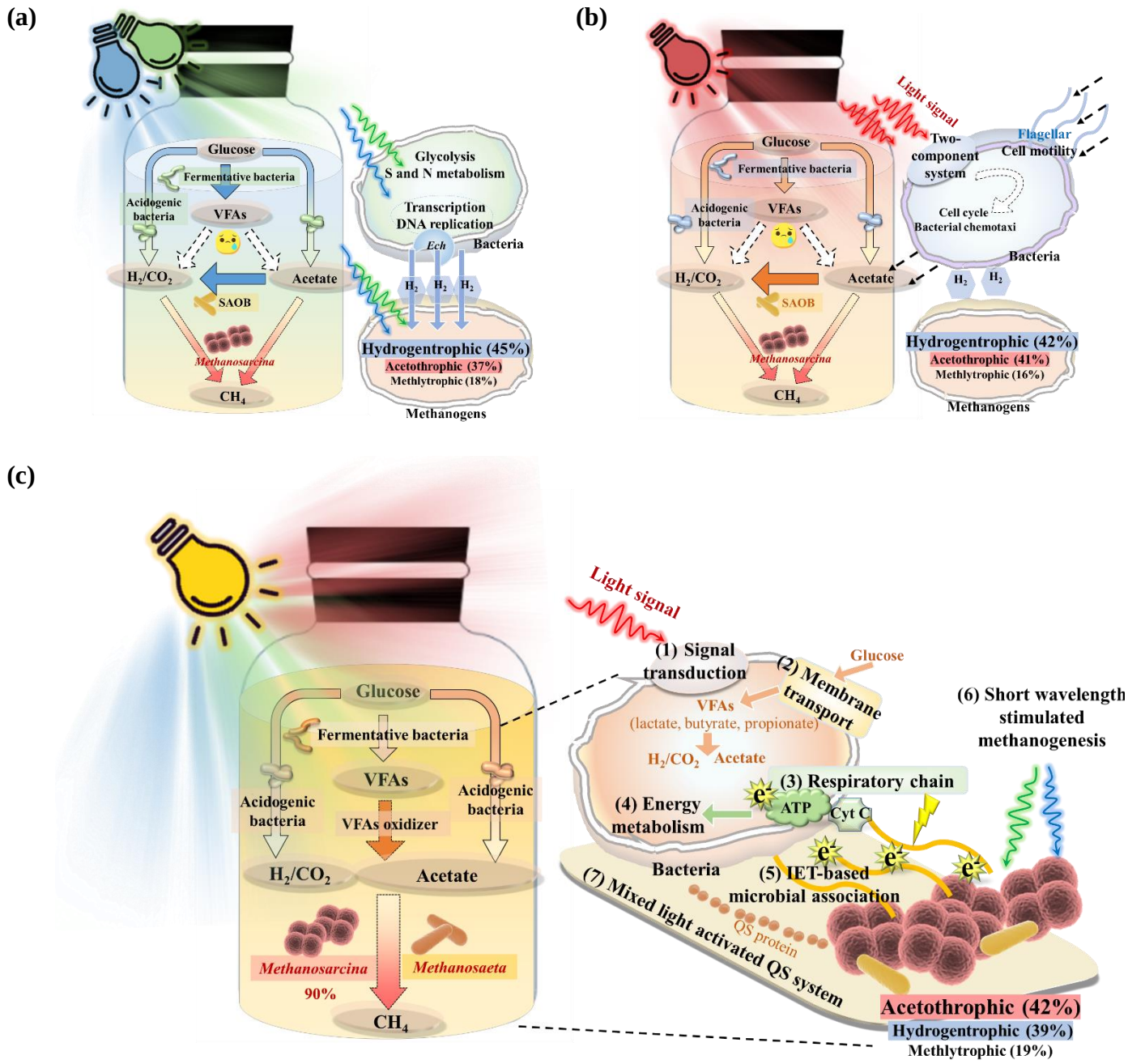

Figure 8